3-14-2014

Multiple Signal Classification for Determining Direction of Arrival of Frequency Hopping Spread Spectrum Signals

Fawwaz Alsubaie

MULTIPLE SIGNAL CLASSIFICATION FOR DETERMINING DIRECTION OF ARRIVAL OF FREQUENCY HOPPING SPREAD SPECTRUM SIGNALS.

THESIS

Fawwaz Alsubaie, First Lieutenant, Royal Saudi Air Force, RSAF

AFIT-ENG-14-M-05

DEPARTMENT OF THE AIR FORCE
AIR UNIVERSITY

AIR FORCE INSTITUTE OF TECHNOLOGY

Wright-Patterson Air Force Base, Ohio

The views expressed in this thesis are those of the author and do not reflect the official policy or position of United States Air Force, Department of Defense, the United States Government, the corresponding agencies of the Saudi Arabian Air Force, the Department of Defense, or the Saudi Arabian Government or any other defense organization.

AFIT-ENG-14-M-05

MULTIPLE SIGNAL CLASSIFICATION FOR DETERMINING DIRECTION OF ARRIVAL OF FREQUENCY HOPPING SPREAD SPECTRUM SIGNALS.

THESIS

Presented to the Faculty

Department of Electrical and Computer Engineering

Graduate School of Engineering and Management

Air Force Institute of Technology

Air University

Air Education and Training Command

in Partial Fulfillment of the Requirements for the

Degree of Master of Science in Electrical Engineering

Fawwaz Alsubaie, B.S.E.E.

First Lieutenant, Royal Saudi Air Force, RSAF

March 2014

AFIT-ENG-14-M-05

MULTIPLE SIGNAL CLASSIFICATION FOR DETERMINING DIRECTION OF ARRIVAL OF FREQUENCY HOPPING SPREAD SPECTRUM SIGNALS.

Fawwaz Alsubaie, B.S.E.E.
First Lieutenant, Royal Saudi Air Force, RSAF

Approved:

//signed//	7 Feb 2014
Richard K. Martin, PhD (Chairman)	Date
//signed//	7 Feb 2014
Maj Mark D. Silvius, PhD (Member)	Date
//signed//	7 Feb 2014
Capt Dustin G. Mixon, PhD (Member)	Date

AFIT-ENG-14-M-05

Abstract

This research extends a multiple signal classification (MUSIC) algorithm to determine direction of arrival (DOA) of frequency hopping spread spectrum (FHSS) signals. All incident FHSS signals have unknown DOA and use phase shift keying (PSK). Conventional MUSIC algorithm involves multiple MUSIC estimation for all frequency bins. On the other hand, the extended development is meant to execute a single MUSIC algorithm of observations on multiple frequency bins or hops. The new extension shows better performance compared to the conventional MUSIC execution at different signal to noise ratio (SNR) levels. Both have the same power accumulation at the true angles of arrival. However, the new development has lower side lobes and hence helps avoid false detections. In addition, the new development has lower side lobes variance resulting in lower error of false detections compared to the normal execution. Simulation results show that the new extension is sensitive to the SNR values and number of samples taken at each frequency bin. However, it is less sensitive to the possible number of frequency hops or *hop set* and number of array sensors.

I dedicate my thesis work to my family and many friends. A special feeling of gratitude to my father whose words of encouragement and push for tenacity ring in my ears. My friends have never left my side and are very special. I also dedicate my work to the Royal Saudi Air Force (RSAF) who gives me this chance to learn, represent and impact the mission and vision of our force.

Table of Contents

Page

Page

List of Figures

List of Tables

List of Acronyms

Acronym	Definition
AWGN	additive white Gaussian noise
BPSK	binary phase shift keying
CR	cognitive radio
CSS	coherent signal subspace
DFT	discrete Fourier transform
DOA	direction of arrival
ED	energy detection
FFH	fast FHSS
FFT	fast Fourier transform
FHSS	frequency hopping spread spectrum
FMD	frequency dependent modeling
LFSR	linear feedback shift register
MATLAB®	matrix laboratory
MTM	multiple taper method
MUSIC	multiple signal classification
MVDR	minimum variance distortionless reposnse
PSK	phase shift keying
QAM	quadrature amplitude modulation
QPSK	quadrature phase shift keying
RS	random sequence
RSS	rotational signal subspace
RV	random variable
SFH	slow FHSS

Acronym	Definition
SNR	signal to noise ratio
SST	signal subspace transformation
SVD	singular value decomposition

MULTIPLE SIGNAL CLASSIFICATION FOR DETERMINING DIRECTION OF ARRIVAL OF FREQUENCY HOPPING SPREAD SPECTRUM SIGNALS.

I. Introduction

This chapter summarizes the research presented in this thesis. Its motivation and goals are explained. Then, the steps taken to develop the thesis are listed. Last, the organization of information and results illustrated in this thesis are presented.

1.1 Research Motivation

Cognitive radio is a promising technology that deals with spectrum scarcity. One application of cognitive radio (CR) is spectrum reuse. To reuse unlicensed spectrum, secondary users (unlicensed users) should ensure the frequency bands are free and no primary user (licensed user) exists [12]. Recent research is looking at spectrum management and the idea of spectrum reuse especially in military environments where the number of white spaces in spectrum is limited [2, 12, 25]. The entire picture is to determine the following features for a given frequency band:

- The existence of a primary user at a given frequency band.
- DOA of all users in the given frequency band.

Many research papers try to improve spectrum hole detection in CR. Recent work examines using multiple taper method (MTM) with singular value decomposition (SVD) to elevate spectral resolution and decrease required computation time [17] . Simulation results show that MTM outperforms conventional energy detection (ED) [1]. With the aid of the research done in the detection part of the spectrum hole detection, one can further look at DOA

angles of present users, another qualifier that adds to a given frequency band status. By defining both existence and direction of a primary user in a given frequency band, spectrum reuse can be more efficient and effective.

1.2 Research Goal

The goal of this thesis is to advance the use of the most popular DOA algorithm for a specific type of communication signals. MUSIC algorithm is a subspace algorithm used to determine DOA of a present primary user at a specific frequency band [16]. In many military applications, FHSS modulation is used to mitigate possible jamming threats. The goal is to extend the algorithm to work for FHSS signals and show the results compared to the iterative MUSIC execusion for all frequencies. Possible affecting factors on the new extension are presented and discussed.

1.3 Research Methodology

First of all, a basic MUSIC algorithm is developed using matrix laboratory (MATLAB®) software to determine DOA of a single user transmitting a tone at a known carrier frequency in a free-noise environment. The result is verified with the true data. Then, additive white Gaussian noise (AWGN) is added to simulate a practical channel effect. The previous steps are processed for more than one user under different SNR levels. This step builds a solid basis to research different user implementations. The previous model is researched under the use of real transmitted bits modulated using binary phase shift keying (BPSK), quadrature phase shift keying (QPSK) and 16-quadrature amplitude modulation (QAM). Therefore, a pre-step was taken to build BPSK, QPSK and 16-QAM modulators in MATLAB®. At first, single user is transmitting using BPSK, QPSK, 16-QAM at a known carrier frequency in a noise-free environment. Then AWGN is added to give a practical flavor to the model. After that, more users were added to the system with various SNR levels transmitting at the same carrier frequency. After that, the research is

steered towards DOA of FHSS signals. Multiple steps have been prepared prior to simulate DOA of FHSS signals. First, a FHSS signal generator based on a pseudo random hopping pattern is built in MATLAB®. Then, a synchronization module is added to make a real FHSS system. The goal of the synchronization is to get the transmitter and the receiver synchronized. Once they get synchronized, an extended MUSIC algorithm is performed to determine angles of arrival of the present users.

1.4 Thesis Outlines

Chapter II introduces the basic theory of the communication modulations considered and describes communication features discussed in the literature such as bandwidth and power. Then, the fundamental MUSIC algorithm theory is presented. Algorithm advantages and limitation are explained. After that, a separate section is dedicated to illustrate the theory of FHSS signals including current types of hopping, hoping sequence generator, practical synchronization procedure, hoping rate and hop set definitions.

Chapter III presents the steps taken to develop DOA of FHSS signals based on the theory explained in Chapter II. First, the process of simulating multiple MUSIC execusion for FHSS signals is performed to build a baseline for later comparison. Then, the new development is introduced to start generating new and fresh results. The new data is compared to the baseline collected previously. After that, multiple parameters are varied to study the effect on the algorithm module such as number of samples, hop set and SNR levels. Finally, a synchronization block is added to simulate a real FHSS system.

Chapter IV provides the simulation results as described in Chapter III. The results are generated many times, averaged and plotted. Figures for the output of the developed MUSIC module are shown. Plots of the output are generated with various parameter values compared to the baseline.

Finally, Chapter V gives a summary of the research with an estimate of its theoretical findings and operational impact. The thesis concludes with a discussion of potential areas for continued research and further testing.

II. Background and Literature Review

This chapter discusses theory and related previous work to this research. The background will address the main theoretical concepts covered in this work. The areas of research include: PSK, FHSS and MUSIC algorithm to estimate DOA. The other side of this chapter briefs related work to MUSIC algorithm to determine DOA of wide-band incident signals.

2.1 Communication Modulation:

This research involves two types of modern communication modulations. PSK is broadly used in current communication technology. The first section gives upper layer background review and concepts of PSK. Then, with the advance of the technology in military applications, FHSS is used in to mitigate possible jamming effects. The FHSS modulation is a crucial part of this research and hence, a sole section is dedicated to address the related theoretical background.

2.1.1 Phase Shift Keying (PSK).

PSK is a digital modulation scheme that conveys data by changing, or modulating, the phase of a reference signal (the carrier wave). Any digital modulation scheme uses a finite number, or M in short, of distinct signals to represent digital data. The set of M different phases assigns a unique pattern of binary digits. Usually, each phase encodes an equal number of bits. Each pattern of bits forms the symbol that is represented by the particular phase. The carrier phase may have one of M values in any symbol period T_{sym} given by:

$$\theta_m = \frac{2\pi}{M}(m-1) \tag{2.1}$$

where $m = 1, 2, \cdots, M$. Therefore, the modulated M-PSK waveform at a carrier frequency is

$$\text{M-PSK}: s_m(t) = A\cos\left(2\pi f_c t + \frac{2\pi}{M}(m-1)\right) \tag{2.2}$$

where $0 \leq t \leq T_{sym}$ and $m = 1, 2, \cdots, M$. From Equation (2.2) we can calculate the transmitted symbols for BPSK, QPSK, 8-PSK and 16-PSK:

$$\text{BPSK}: s_m(t) = A\cos\left(2\pi f_c t + (m-1)\pi\right) \qquad m = 1, 2 \tag{2.3a}$$

$$\text{QPSK}: s_m(t) = A\cos\left(2\pi f_c t + \frac{\pi}{2}(m-1)\right) \qquad m = 1, 2, 3, 4 \tag{2.3b}$$

$$\text{8-PSK}: s_m(t) = A\cos\left(2\pi f_c t + \frac{\pi}{4}(m-1)\right) \qquad m = 1, 2, \cdots, 8 \tag{2.3c}$$

$$\text{16-PSK}: s_m(t) = A\cos\left(2\pi f_c t + \frac{\pi}{8}(m-1)\right) \qquad m = 1, 2, \cdots, 16 \tag{2.3d}$$

Figure 2.1 shows different PSK constellation diagrams where $\phi_1(t)$ and $\phi_2(t)$ are the two orthognal trigonometric functions: $\cos(2\pi f_c t)$ and $\sin(2\pi f_c t)$, respectively.

2.1.2 Frequency Hopping Spread Spectrum.

This section discusses some of the features of FHSS. First, a brief background is given to identify basic FHSS terms and definitions. Then, coherent and non-coherent detection is illustrated. The difference between fast FHSS (FFH) and slow FHSS (SFH) is explained later. Finally, a sole section is dedicated to describe the process of code generation of FHSS signals.

2.1.2.1 Background.

FHSS is a method of transmitting radio signals on multiple carriers. The carrier switches among many channels or a hop set. The switching pattern is controlled by LFSR sequences. The transmitter and the receiver share the sequence during the synchronization phase. When the transmitter and the receiver get synchronized, they start a communication session or get to a sleep mode. Figure 2.2 illustrates the process.

In the synchronization phase, the transmitter starts sending the synchronization packet hopping between one of the frequency channels. The synchronization packet is unlikely to occur in the communication mode. Therefore, the receiver can identify the occurrence of synchronization. The receiver listens on one of the frequency channels. The receiver

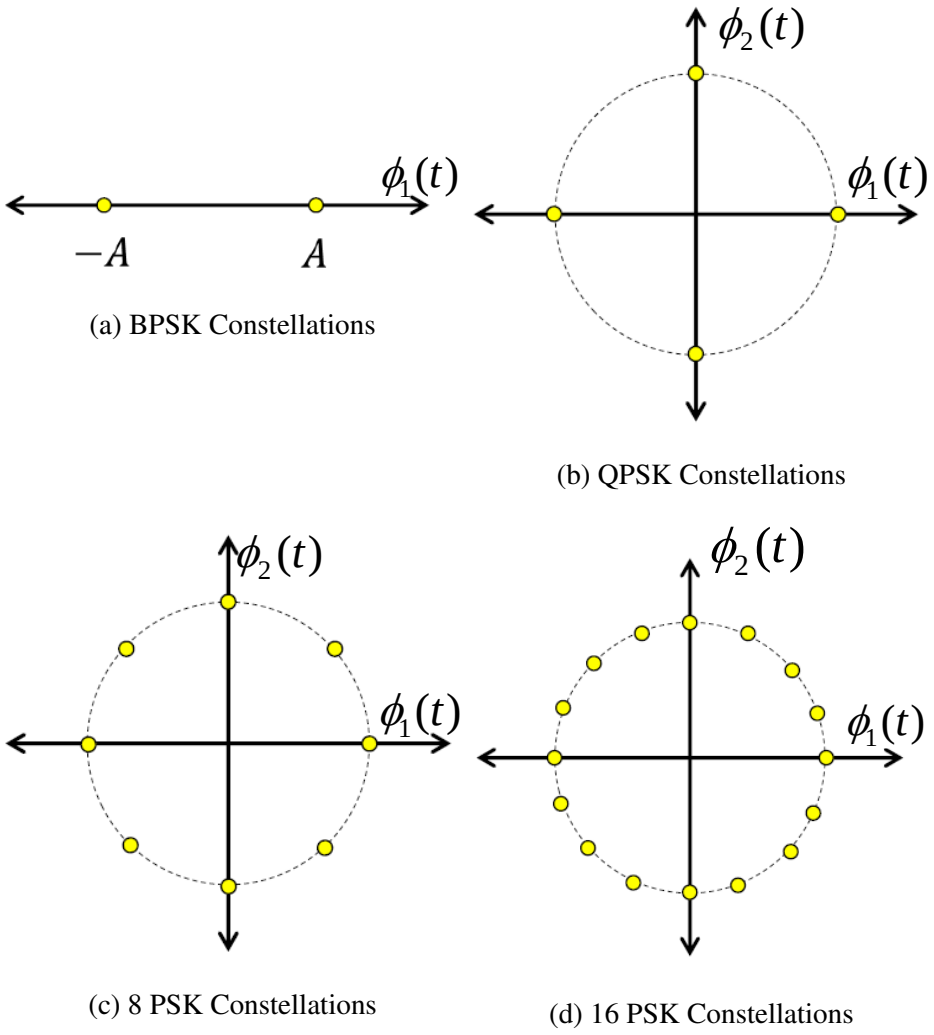

(a) BPSK Constellations

(b) QPSK Constellations

(c) 8 PSK Constellations

(d) 16 PSK Constellations

Figure 2.1: Communication Constellations.

channel is chosen arbitrarily and independently from the transmitter. If the receiver channel happens to be one of the channel destinations of the receiver, the synchronization usually takes place. The transmitter keeps sending the synch packet untill it receives an acknowledgment. As SNR decreases, the synchronization process starts to be ambiguous [19].

2.1.2.2 FHSS Detection.

There are two types of FHSS signals detection:

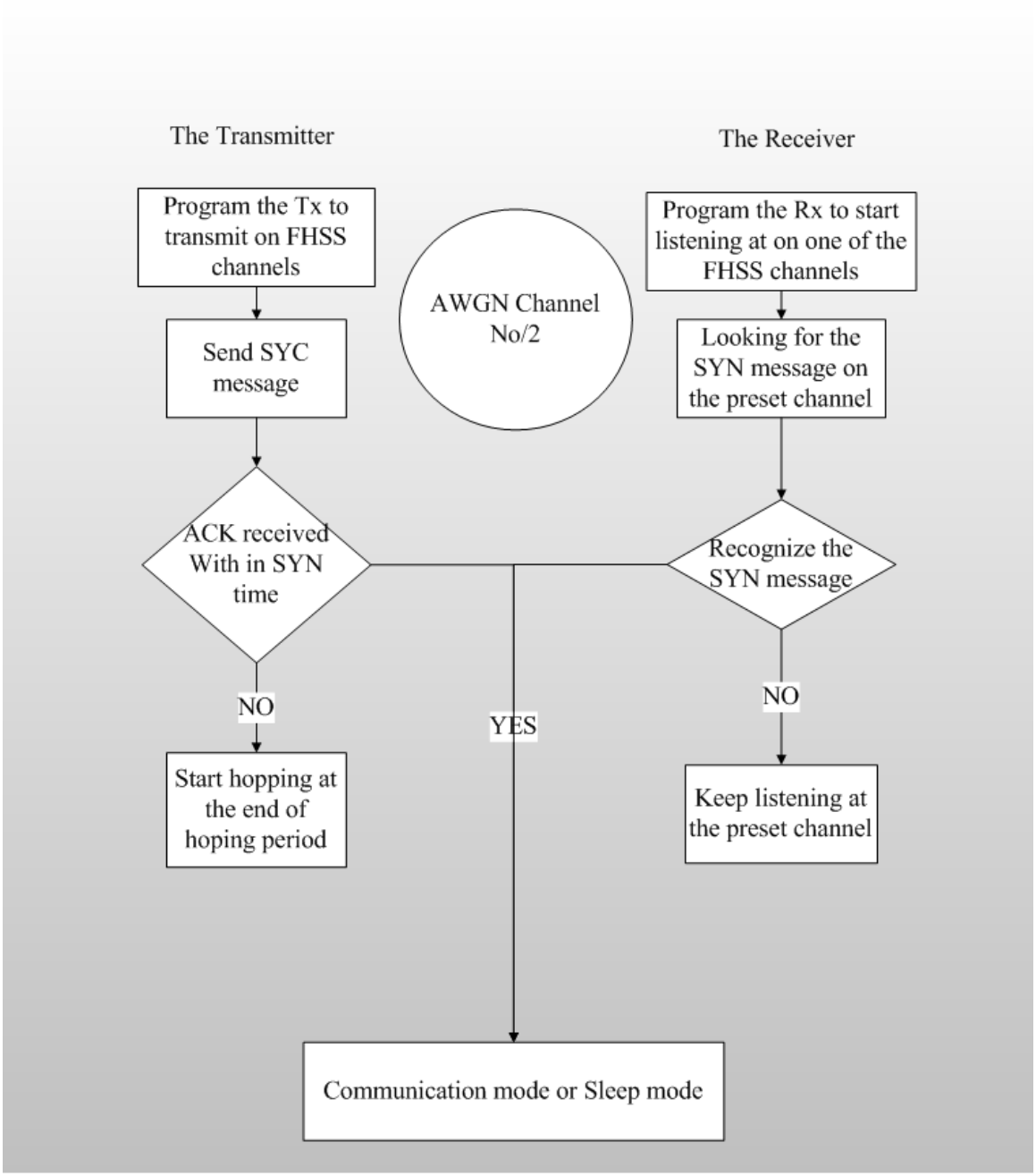

Figure 2.2: Two steps communication for FHSS systems.

- Coherent detection, also referred to as coherent demodulation, is a technique of phase locking to the carrier wave to improve detection. Knowledge of the carrier phase improves demodulator performance. Therefore, to demodulate FHSS signals, the

receiver has to estimate the carrier frequency which turns out to be cumbersome. For coherent detection, the orthogonality of FHSS frequency channels leads to a condition of tone spacing given by [20]:

$$2\pi(f_2 - f_1)T_{sym} = k\pi$$

or

$$f_2 - f_1 = \frac{k}{2T_{sym}}$$

therefore,

$$f_{min} = \frac{1}{2T_{sym}}$$

where:

T_{sym} is symbol duration in *sec*.

k is an integer constant.

f_1 and f_2 are two consecutive FHSS frequency channels in Hz.

f_{min} is the minimum spectral speration of FHSS freqeuncy channels in Hz.

- Non-coherent detection, is a common practice to detect FHSS carrier frequency and does not require carrier phase estimation. It is a method to utilize the envelope of the received waveform to approximate the shape of the signal. This research generates FHSS signals assuming non-coherent detection implementation. For non-coherent detection of FHSS carrier frequencies, the orthogonality condition leads to a minimum tone spacing of $1/T_{sym}$.

2.1.2.3 Fast and Slow Frequency Hopping.

In frequency hopping systems, the transmitter changes the carrier frequency according to a certain hopping pattern. The advantage is that the signal sees a different channel and a different set of interfering signals during each hop. This avoids the problem of failing

communication at a particular frequency, because of a fade or a particular interferer. The FHSS system theoretically hops between frequency channels. The shortest duration of a tone is called a chip, T_c. The FHSS systems are classified according to their hopping characteristics to:

- Slow frequency hopping SFH: In this case one or more data bits are transmitted within one hop. An advantage is that coherent data detection is possible. Often, systems using slow hopping also employ (burst) error control coding to restore loss of (multiple) bits in one hop. The chip rate R_c in SFH systems is less than or equal to the symbol rate R_s resulting in a net bandwidth of:

$$BW_{SFH} = (M + 1)R_c \tag{2.4}$$

where M is the number of possible hopping channels. Figure 2.3 shows a SFH hopping pattern.

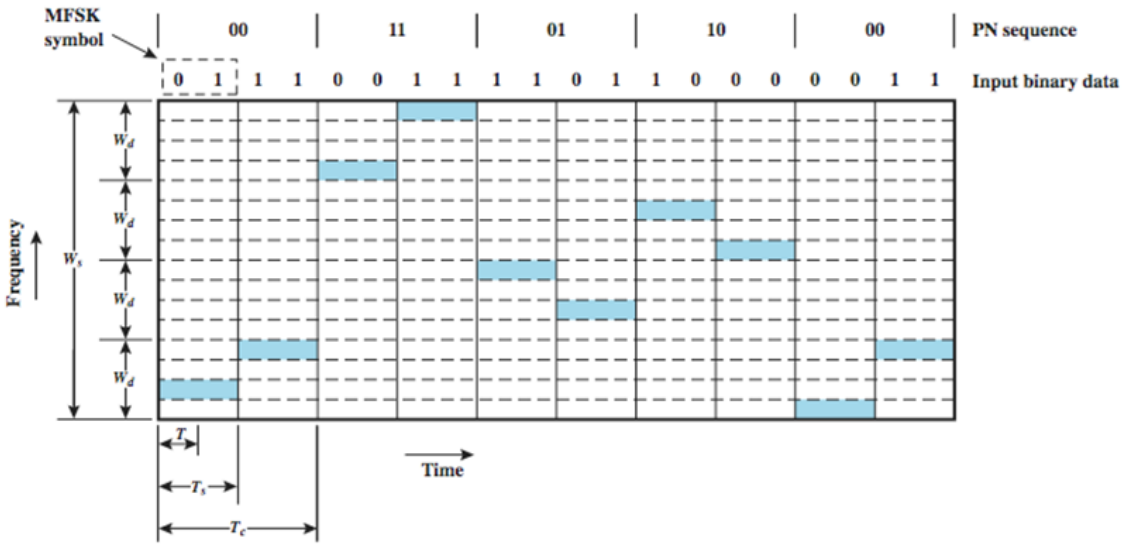

Figure 2.3: Slow frequency hopping [21].

This research implements SFH system in MATLAB® to simulate FHSS signals.

- Fast frequency hopping FFH: one data bit is divided over multiple hops. In fast hopping, coherent signal detection is difficult, and seldom used. The required bandwidth for FFH systems is larger compared to SFH system:

$$BW_{FFH} = (M + 3)\frac{R_c}{2} \tag{2.5}$$

where M is the number of possible hopping channels. Figure 2.4 shows a FFH hopping pattern.

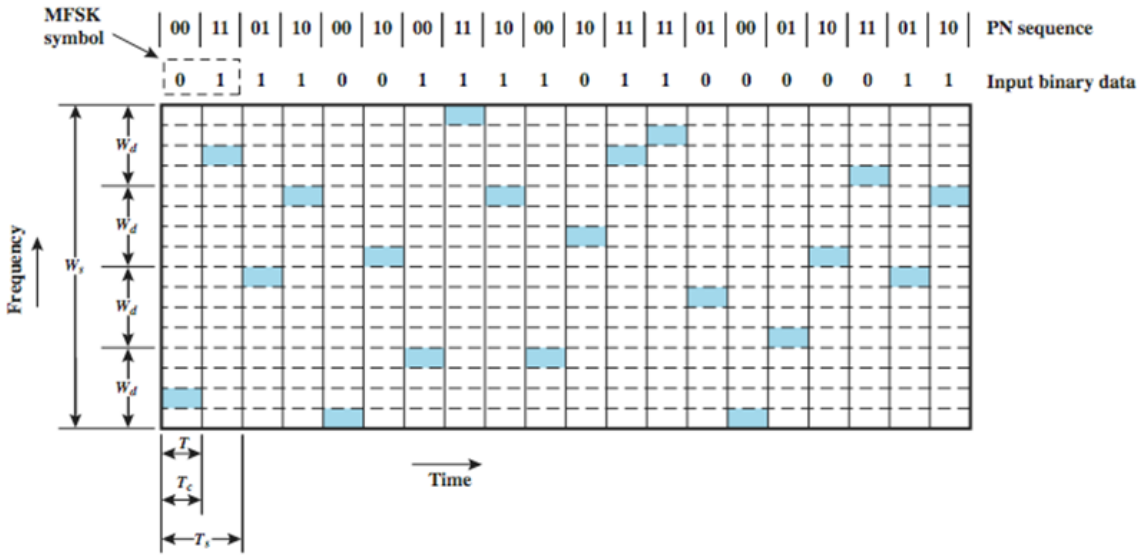

Figure 2.4: Fast frequency hopping [21].

2.1.2.4 FHSS Code Generation.

As mentioned above, frequency hopping systems implement a code generator to pseudo-randomly generate sequences to control the frequency hopping pattern. random sequence (RS) are compared by certain properties such as: periodic correlation, code cycle, randomness and implementation. This project implements LFSR sequences to determine the hopping pattern. LFSR is a shift register whose input bit is a linear function of its previous state. The number of shift register (L) in LFSR unit is called "stages." The most

commonly used linear function of single bits is a $mod-2$ adder. Thus, an LFSR is most often a shift register whose input bit is driven by the $mod-2$ adder of some bits of the overall shift register value. Figure 2.5 shows a three-stage LFSR sequence generator with $mod-2$ adder:

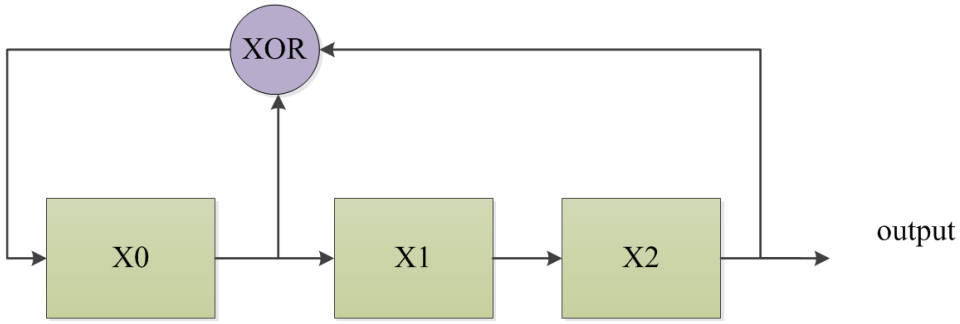

Figure 2.5: Three-stage LFSR sequence generator [20].

The initial value of the LFSR is called the seed, and because the operation of the register is deterministic, the stream of values produced by the register is completely determined by its current (or previous) state. Likewise, because the register has a finite number of possible states, it must eventually enter a repeating cycle of length $2^L - 1$. However, an LFSR with a well-chosen feedback function can produce a sequence of bits which appears random and has a very long cycle. Table 2.1 illustrates a three-stage LFSR state transition.

2.2 Mulitple Signal Classification (MUSIC)

MUltiple **SI**gnal **C**lassication (MUSIC) is the most popular technique used in DOA estimation. We can summarize DOA estimation as the work of estimating the direction of an unknown incoming signal to a receiver antenna by some processing techniques.

Table 2.1: State transition table.

State	Current state	Next State
1	001	100
2	100	010
3	010	101
4	101	110
5	110	111
6	111	011
7	011	001

2.2.1 MUSIC Method.

The MUSIC method is a relatively simple and efficient eigenstructure method of DOA estimation. It has many variations and is perhaps the most studied method in its class. In its standard form, also known as spectral MUSIC, the method estimates the noise subspace from available samples. This can be done by either eigenvalue decomposition of the estimated array correlation matrix or singular value decomposition of the data matrix, with its columns being the snapshots of the array signal vectors. The latter is preferred for numerical reasons. Once the noise subspace has been estimated, a search for angle pairs in the range is made by looking for steering vectors that are as orthogonal to the noise subspace as possible. This is normally accomplished by searching for peaks in the MUSIC spectrum.

2.2.2 Data Model.

If there are D signals incident on the array, the N received input data vector at the m^{th} element array, $\underline{X}_m(t) \in \mathbb{C}^{1\times N}$, can be expressed as a linear combination of the incident waveforms and noise. That is,

$$\underline{X}_m(t) = \sum_{l=0}^{l=D-1} a_m(\theta_l)\underline{s}_l(t) + \underline{w}(t) \tag{2.6}$$

or for all M-element array, the received matrix $\mathbf{X}(t) \in \mathbb{C}^{M\times N}$:

$$\mathbf{X}(t) = \begin{bmatrix} \underline{X}_1^T(t) \\ \underline{X}_2^T(t) \\ \vdots \\ \underline{X}_M^T(t) \end{bmatrix} \tag{2.7}$$

$$\mathbf{X}(t) = \begin{bmatrix} \underline{a}(\theta_0) & \underline{a}(\theta_1) & \cdots & \underline{a}(\theta_{D-1}) \end{bmatrix} \begin{bmatrix} \underline{s}_0^T(t) \\ \underline{s}_1^T(t) \\ \vdots \\ \underline{s}_{D-1}^T(t) \end{bmatrix} + \mathbf{W}(t) \tag{2.8}$$

or,

$$\mathbf{X}(t) = \mathbf{A}\mathbf{S}(t) + \mathbf{W}(t) \tag{2.9}$$

where:

$\mathbf{S}(t) \in \mathbb{R}^{D\times N}$ is the matrix of incident signals' vectors.

$\mathbf{W}(t) \in \mathbb{C}^{M\times N}$ is the noise matrix.

$\mathbf{A} \in \mathbb{C}^{M\times D}$ is the array steering matrix.

$\underline{a}(\theta_j) \in \mathbb{C}^{M\times 1}$ is the array steering vector corresponding to the DOA of the j^{th} signal.

For simplicity, we will drop the time arguments from $\mathbf{X}$, $\mathbf{S}$ and $\mathbf{W}$ from this point onwards. In geometric terms, at the instant n, the received vector $\underline{X}_n$ and the steering vectors $\underline{a}(\theta_j)$ can be visualized as vectors in M dimensional space. From Equation (2.8), it is seen that $\underline{X}_n$ is a particular linear combination of the array steering vectors $\underline{a}(\theta_j)$, with $s_0(n)$,$s_1(n)$,$\cdots$,$s_{D-1}(n)$ being the coefficients of the combination. In terms of the above data model, the input covariance matrix $\mathbf{R}_{xx} \in \mathbb{C}^{M\times M}$ can be expressed as

$$\mathbf{R}_{xx} = \mathbf{A}\mathbf{E}[\mathbf{S}\mathbf{S}^H]\mathbf{A}^H + \mathbf{E}[\mathbf{W}\mathbf{W}^H] \tag{2.10}$$

$$\mathbf{R}_{xx} = \mathbf{A}\mathbf{R}_{ss}\mathbf{A}^H + \mathbf{R}_{nn} \tag{2.11}$$

where:

$\mathbf{R}_{ss} \in \mathbb{R}^{D\times D}$ is the signal correlation matrix $\mathbf{E}[\mathbf{S}\mathbf{S}^H]$.

$\mathbf{R}_{nn} \in \mathbb{C}^{M\times M}$ is the noise correlation matrix $\mathbf{E}[\mathbf{W}\mathbf{W}^H]$.

Assuming uncorrelated AWGN

$$\mathbf{R}_{xx} = \mathbf{A}\mathbf{R}_{ss}\mathbf{A}^H + \sigma_n^2\mathbf{I} \tag{2.12}$$

The eigenvalues of $\mathbf{R}_{xx}$ are the values $\lambda_0, \lambda_1, \cdots, \lambda_{D-1}$ such that:

$$|\mathbf{R}_{xx} - \lambda_i\mathbf{I}| = 0 \tag{2.13}$$

Using Equation (2.12) :

$$\left|\mathbf{A}\mathbf{R}_{ss}\mathbf{A}^{\mathbf{H}} + \sigma_n^2\mathbf{I} - \lambda_i\mathbf{I}\right| = \left|\mathbf{A}\mathbf{R}_{ss}\mathbf{A}^{\mathbf{H}} - (\lambda_i - \sigma_n^2)\mathbf{I}\right| = \mathbf{0} \tag{2.14}$$

Therefore, the eignvalues of, v_i of $\mathbf{A}\mathbf{R}_{ss}\mathbf{A}^{\mathbf{H}}$ are:

$$v_i = \lambda_i - \sigma_n^2 \tag{2.15}$$

Since $\mathbf{A}$ is comprised of steering vectors which are linearly independent, it has full column rank, and the signal correlation matrix $\mathbf{R}_{ss}$ is non-singular as the incident signals are not highly correlated. A full column rank $\mathbf{A}$ matrix and non-singular $\mathbf{R}_{ss}$ guarantees that, when the number of incident signals D is less than the number of array elements M, the $M \times M$ matrix $\mathbf{A}\mathbf{R}_{ss}\mathbf{A}^H$ is positive semi-definite with rank D. From elementary linear algebra, this implies that $M - D$ of the eignvalues, v_i , of $\mathbf{A}\mathbf{R}_{ss}\mathbf{A}^H$ are zero. From equation Equation (2.15), this means that $M - D$ of the eignvalues of R_{xx} are equal to the noise variance σ_n^2 . We then sort the eignvalues of $\mathbf{R}_{xx}$ such that λ_0 is the largest eignvalue, and λ_{M-1} is the smallest eignvalue. Therefore,

$$\lambda_D, \cdots, \lambda_{M-1} = \sigma_n^2 \tag{2.16}$$

In practice, however, when the autocorrelation matrix $\mathbf{R}_{xx}$ is estimated from a finite data sample, all the eigenvalues corresponding to the noise power will not be identical. Instead they will appear as a closely spaced cluster, with the variance of their spread decreasing as the number of samples used to obtain an estimate of $\mathbf{R}_{xx}$ is increased. Once the multiplicity, K, of the smallest eigenvalue is determined, an estimate of the number of signals, $\hat{D}$, can be obtained by Equation (2.17).

$$\hat{D} = M - K \tag{2.17}$$

In this research, the number of incident signals D is known. The eigenvector $\underline{q}_i$ associated with a particular eigenvalue λ_i is the vector such that

$$\mathbf{R}_{xx} - \lambda_i \mathbf{I} = 0 \tag{2.18}$$

For eigenvectors associated with the $M - D$ smallest eigenvalues, we have

$$(\mathbf{R}_{xx} - \sigma_n^2 \mathbf{I})\underline{q}_i = \mathbf{A}\mathbf{R}_{ss}\mathbf{A}^H \underline{q}_i + \sigma_n^2 \mathbf{I} - \sigma_n^2 \mathbf{I} = \underline{0} \tag{2.19}$$

$$\mathbf{A}\mathbf{R}_{ss}\mathbf{A}^H \underline{q}_i = \underline{0} \tag{2.20}$$

Since $\mathbf{A}$ has full rank and $\mathbf{R}_{ss}$ is non-singular, this implies that

$$\mathbf{A}^H \underline{q}_i = \underline{0} \tag{2.21}$$

$$\begin{bmatrix} \underline{a}^H(\theta_0)\underline{q}_i \\ \underline{a}^H(\theta_1)\underline{q}_i \\ \vdots \\ \underline{a}^H(\theta_{D-1})\underline{q}_i \end{bmatrix} = \begin{bmatrix} 0 \\ 0 \\ \vdots \\ 0 \end{bmatrix} \tag{2.22}$$

This means that the eigenvectors associated with the $M - D$ smallest eigenvalues are orthogonal to the D steering vectors that make up $\mathbf{A}$.

$$\{a(\theta_0), \cdots\cdots\cdots, a(\theta_{D-1})\} \perp \{q_D, \cdots\cdots\cdots, q_{M-1}\} \tag{2.23}$$

This is the essential observation of the MUSIC approach. It means that one can estimate the steering vectors associated with the received signals by finding the steering vectors which are most nearly orthogonal to the eigenvectors associated with the eigenvalues of $\mathbf{R}_{xx}$ that are approximately equal to σ_n^2 .

This analysis shows that the eigenvectors of the covariance matrix $\mathbf{R}_{xx}$ belong to either of the two orthogonal subspaces, called the principle eigensubspace (signal subspace) and the non-principle eigensubspace (noise subspace). The steering vectors corresponding to the DOA lie in the signal subspace and are hence orthogonal to the noise subspace. By searching through all possible array steering vectors to find those which are perpendicular to the space spanned by the non-principle eigenvectors, the DOA can be estimated. To search the noise subspace, we form a matrix $\mathbf{U}_n \in \mathbb{C}^{M\times M-D}$ containing the noise eigenvectors:

$$\mathbf{U}_n = \begin{bmatrix} \underline{q}_D & \underline{q}_{D+1} & \cdots & \cdots & \cdots & \underline{q}_{M-1} \end{bmatrix} \tag{2.24}$$

Since the steering vectors corresponding to signal components are orthogonal to the noise subspace eigenvectors, $\underline{a}^H(\hat{\theta})\mathbf{U}_n\mathbf{U}_n^H\underline{a}(\hat{\theta})$ for $\hat{\theta}$ corresponding to the DOA of a multipath component. Then the DOAs of the multiple incident signals can be estimated by locating the peaks of a MUSIC spatial spectrum given by:

$$P_{MUSIC}(\hat{\theta}) = \frac{1}{\underline{a}^H(\hat{\theta})\mathbf{U}_n\mathbf{U}_n^H\underline{a}(\hat{\theta})} \tag{2.25}$$

The orthogonality between the noise subspace and the steering vectors will minimize the denominator and hence will give rise to peaks in the MUSIC spectrum defined in Equation (2.25). The largest peaks in the MUSIC spectrum correspond to the signals impinging on the array.

2.3 Research on Wideband Source Location Using MUSIC Algorithm

In recent applications, the demand of high data rate generally tends to drive more bandwidth occupation. Therefore, researchers have been looking at determining wideband

source locations and yet retain estimator accuracy. This research is directed towards the MUSIC algorithm and hence will discuss efforts related to wideband source location techniques using the MUSIC algorithm. In the wideband case, the location problem can be regarded as the simultaneous solution for a set of spatial estimation problems, corresponding to all frequencies in the band. There are several ways to treat this problem, as listed in the next few sections.

2.3.1 Incoherent Approach.

The spatial estimation can be performed independently at all frequencies. The information collected at the various frequencies has then to be aggregated. Since the signal values at different frequencies are independent, the aggregation is incoherent and does not reduce the variance of the estimate. Therefore, the estimate requires a rather large number of snapshots for the estimation of each correlation matrix [5, 24]. Moreover, the incoherent approach performance degrades at low SNR values [5, 24].

2.3.2 Coherent Approach.

According to the viewpoint of signal subspace, the direction vectors at a given frequency f form a signal subspace. Therefore, wideband sources can consist of multiple signal subspaces. The eigenvectors of the noise subspace are functions of frequency f. The main idea of coherent signal subspace (CSS) is to focus or transform signal subspaces of narrow-band components of a wide-band signal to a single signal subspace across a common frequency band f_0. In other words, CSS means merging all signal subspaces to one single signal subspace around f_0. Unlike the incoherent methods, the coherent processing methods can handle perfectly correlated sources. The main task to perform CSS is to come up with a transformation function (or focusing matrix) as a function of frequency to project the steering vector matrix $\mathbf{A}(f_i)$ to $\mathbf{A}(f_0)$ and hence the correlation matrix $\mathbf{R}_{xx}(f_i)$ to $\mathbf{R}_{xx}(f_0)$. Focusing matrix design vastly affects the final estimation accuracy and robustness of the

algorithm. Actually, the first step in designing focusing matrices is the determination of focusing angles in the neighborhood of the true DOA. Those angles could be in:

- Single group: all focusing angles are within one beam width.
- Multi-group: focusing angles are within different beam widths.

The following subsections give a glance at a few focusing matrices used in developing wideband source location estimation using the MUSIC algorithm.

2.3.2.1 Non-unitary Diagonal Matrices.

In [23], the array output matrix $\mathbf{X}$ is first decomposed in temporal domain to a set of k subintervals. For every subinterval k, discrete Fourier transform (DFT) is computed using J-points fast Fourier transform (FFT). The correlation matrix $\mathbf{R}_{xx}(f_i)$ is computed for all J-points. In addition, a set of preliminary angles are estimated using spatial periodogram. After that, the non-unitary diagonal focusing matrix $\mathbf{T}(f_i) \in \mathbb{C}^{M\times M}$ is applied for every correlation matrix $\mathbf{R}_{xx}(f_i)$ and $\mathbf{R}_{nn}(f_i)$ to project them to a single correlation matrix, or coherent matrix, $\mathbf{R}_{xx}(f_0)$ and $\mathbf{R}_{nn}(f_0)$ around f_0. The eigenvalues and eigenvectors of the matrix pencil ($\mathbf{R}_{xx}(f_0)$, $\mathbf{R}_{nn}(f_0)$) are computed. Using the later step, the noise subspace of the coherent matrix $\mathbf{R}_{xx}(f_0)$ is determined. At this point, using the coherent matrix $\mathbf{R}_{xx}(f_0)$ and the coherent noise subspace, normal MUSIC algorithm can performed to estimate DOA.

2.3.2.2 Rotational Signal Subspace (RSS).

The method in [13] introduces a class of focusing matrices rotational signal subspace (RSS) to implement CSS better than the non-unitary focusing matrices such as the ones used by [23]. The RSS rotates the signal subspace of steering matrix at f_j, $\mathbf{A}(f_j, \theta)$, to match the signal subspace of $\mathbf{A}(f_0, \theta)$ without changing the spatial noise correlation. According to the simulation results in [23], RSS has better estimator accuracy. The method claims to have no focusing loss which is an annihilation effect in SNR value after the focusing

process. The drawback of the RSS focusing matrix is the computational burden because of the rotation process.

2.3.2.3 Signal Subspace Transformation (SST).

The approach in [8] implements CSS using signal subspace transformation (SST) focusing matrices to generate a sufficient statistics of the correlation matrix $\mathbf{R}_{xx}$. RSS presented in reference [13] is a special case of SST. The goal behind SST is to reduce the computations in RSS method by about 10 and yet maintain the same estimator accuracy.

Some researchers have examined prior work to the focusing process. In [9], the authors claim the existence of a set of orthogonal basis functions that span the noise subspace. Those basis functions are frequency dependent. The Kronecker products of those functions and noise vector $\underline{w}(t)$, signal vector $\underline{s}(t)$ and received vector $\underline{X}(t)$ are computed. The resultant matrix has larger size and more extended resulting in expressing the noise subspace effectively more the normal CSS. After that, focusing matrices (unitary, rotational, diagonal) are applied to the extended $\mathbf{X}$ to focus the signal subspaces to a single signal subspace. Results show that this step adds more resolution probability at low SNR levels.

2.3.3 The Temporo-Spatial Approach.

Schmidt's approach for DOA narrow band signals is high resolution and works for correlated signals [18]. The idea is that the steering matrix $\mathbf{A}$ has $M \times D$ size and always has a maximum rank of D. The column space of $\mathbf{A}$ is called the signal subspace and the columns of $\mathbf{A}$ are members of the column space. The matrix $\mathbf{A}$ is a function of the DOA and frequency f. The MUSIC idea is to project any steering vector to the orthogonal complement (noise subspace). If the projection is zero, that means there exists a primary user. Alternatively, the noise subspace is the null space of the correlation matrix $\mathbf{R}_{xx}$ (or the eigenvector corresponding to minimum eigenvalues of $\mathbf{R}_{xx}$) and the signal subspace could be defined as the eigenvectors corresponding to maximum eigenvalues of $\mathbf{R}_{xx}$. Since $\mathbf{R}_{xx}$

is always a full rank matrix, it cannot be used to distinguish between signal subspace and noise subspace and that is why we resort to eigenvalues and eigenvectors. If the signals are wideband, the columns of $\mathbf{A}$ start to vary with frequency and hence the signal subspace changes as well. In fact, the eigenvalues of $\mathbf{R}_{xx}$ begin to be close to each other for wideband incident signals. In [7], the simulated $\mathbf{R}_{xx}$ is calculated. The noise subspace (or null subspace) is defined to be the set of eigenvectors whose eigenvalues are within a specific cluster. The signal subspace of $\mathbf{R}_{xx}$ is the union of the signal subspaces of the narrow band components. Similarly, the noise subspace of $\mathbf{R}_{xx}$ is the intersection of noise subspaces of the narrow band components. The idea is to come up with a correlation matrix $\mathbf{R}_c(\theta)$ for a single signal and then project it on to the noise subspace of $\mathbf{R}_{xx}$. If the projection is zero, then θ is a DOA. Restrictions to this method include: the effect of noise, how to determine the null space (noise subspace) of $\mathbf{R}_{xx}$, how to accurately obtain the signal power spectra and prior knowledge of the source correlation matrix.

2.3.4 Frequency Dependent Modeling (FMD).

Frequency dependent modeling (FMD) introduces basis functions into the array output signal to process the wideband signal. The method proposed in [10] and [6] allow determining DOA of wideband sources in the frequency domain, by combining the information obtained at various frequencies. The correlation matrix of the received signal is expanded using certain basis functions. The basis functions are frequency-dependent. The expanded matrix is diagonalized to determine the minimum eigenvalues corresponding to noise eigenvectors. Finally, the MUSIC algorithm is used to estimate bearing angles.

2.3.5 Rational Estimation.

The 1-D signal subspace approach assumes that the source bandwidths are sufficiently narrow that the array response to a source can be represented as multiplication of the source signal by a complex p-dimensional vector, where p is the number of sensors. The method proposed in [22] is a generalization of the 1-D signal subspace approach to rational vector

space or Z-domain. The correlation matrix is first estimated and then transferred to Z-domain. The rational signal subspace approach allows for variation in sensor spatial and frequency response, array configuration, noise spectral characteristics and correlation. The method performs well for low SNR is capable of locating overlapping spectra has high resolution and is robust for correlated sources. The drawback of this method comes from its computational burden.

2.4 The New MUSIC Development

The thesis work focuses on estimation of DOA of FHSS signals. The goal is to achieve an accurate DOA estimate compared to the existing wide-band estimation methods. The methods discussed in the last few sections suffer from heavy computational burden. In addition, some of them have focusing loss or SNR degradation as in RSS method. Others need prior knowledge of the source correlation matrix $\mathbf{R}_{ss}$ or prior DOA estimation.
This work tries to minimize the computational size involved to perform MUSIC algorithm to estimate DOA and yet obtain an accurate estimate. The new development is meant to outperform the conventional MUSIC algorithm done separately for all possible hopping frequency bins. Moreover, it needs to have a similar computational burden to the conventional MUSIC execution.

III. Methodology

This chapter details the methodology used to develop and test MUSIC to determine DOA of FHSS signals using one time MUSIC process for all hopped frequency bins. Section 3.1 illustrates the process of simulating in MATLAB® the multiple MUSIC algorithm for all frequency bins or *single frequency algorithm* for short. This step comprises a baseline for later comparison. System layout overview, flow chart, and parameters used are presented. Later, the new method is simulated for FHSS algorithm. The new design overview and proposed flow chart along with parameters used are provided in Section 3.2. Data is collected from the later model and compared to the single frequency algorithm results. Section 3.3 presents the metrics used to assess the new development.

3.1 Single Frequency MUSIC Algorithm

This section describes the steps taken to simulate multiple MUSIC algorithm in MATLAB® for FHSS signals. First, the system layout overview and flow chart are shown. Then a table of parameters is provided.

3.1.1 System Layout.

Figure 3.1 shows the system layout for an existing DOA problem. The D users transmit FHSS signals. They continuously transmit and hop between pre-defined frequency channels. This research is directed to all cases users may have except the ambiguous cases mentioned in [18]:

- *Type I*: Two or more received signals have identical incident angles $a(\theta_1) = a(\theta_2)$.
- *Type II*: The continuum of $a(\theta)$ intersects signal subspace more than D times.

According to Figure 3.1, incident stationary signals fall on an array of M sensors. The sensors are equally spaced with distance d. Data is collected and forwarded to the MUSIC

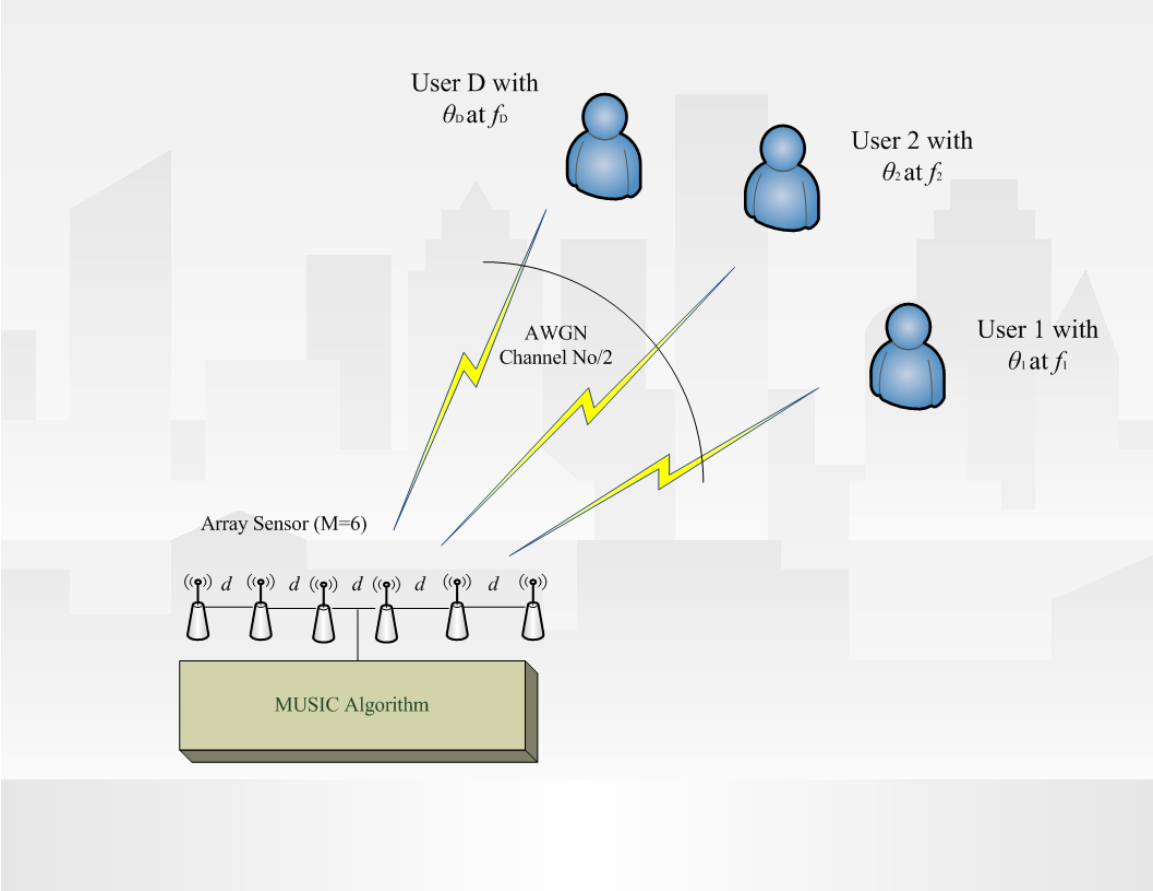

Figure 3.1: Single frequency MUSIC algorithm DOA problem.

block where DOA is estimated. The next section shows the flow chart implemented inside the MUSIC block shown in Figure 3.1.

3.1.2 MUSIC Process Description.

Figure 3.2 shows the procedure followed to determine the DOA of a signal at a certain carrier frequency. The flow chart in Figure 3.2 implements the procedure in most MUSIC algorithm research papers [3, 15, 18]. First, the number of sources can be one or more. In this research, all sources are stationary which can represent for instance a stationary satellite with respect to the receiver on the ground. The M sensors each receive a delayed copy of the incident signal(s) with respect to a reference sensor. The $\mathbf{X}$ matrix defined in Chapter

II is a function of the incident signal(s) vectors, center frequency, incident angle(s) and number of sensors M. The matrix $\mathbf{X}$ represents the received incident signals. Each i^{th} row represents received signal at the i^{th} sensor. The autocorrelation matrix $\mathbf{R}_{xx} \in \mathbb{C}^{M\times M}$ of $\mathbf{X}$ is computed in MATLAB®. The matrix $\mathbf{R}_{xx}$ conveys the correlation between rows of $\mathbf{X}$. Then, the eigenvalues and the eignvectors of $\mathbf{R}_{xx}$ are computed in MATLAB®. Theoretically, number of eigenvectors associated with the signal subspace equals the number of primary users D [18]. Knowing number of primary users D and number of sensors M, the matrix $\mathbf{U}_n \in \mathbb{C}^{M\times M-D}$ can be formed. The matrix $\mathbf{U}_n$ consists of the set of eigenvectors associated with the noise subspace. The matrix $\mathbf{U}_n$ comprises of the eigenvectors whose eignvalues λ_{min} are the variance of the noise . In MATLAB®, λ_{min} occurs in a cluster rather than a precise value. The spread of this cluster decreases with more data processed. The matrix $\mathbf{U}_n$ is orthogonal to the columns of the array steering matrix $\mathbf{A}$ defined in chapter II. After that, steering vectors $\underline{v}(\theta) \in \mathbb{C}^{1\times M}$ are generated for all angles θ between 0 and $\frac{\pi}{2}$:

$$P^{-1}(\theta) = \underline{v}(\theta)\mathbf{U}\mathbf{U}^H\underline{v}^H(\theta). \tag{3.1}$$

or

$$P(\theta) = \frac{1}{\underline{v}(\theta)\mathbf{U}\mathbf{U}^{\mathbf{H}}\underline{v}^H(\theta)}. \tag{3.2}$$

If a given $\underline{v}(\theta)$ is orthogonal to $\mathbf{U}_n$, that $\underline{v}(\theta)$ contains an angle of a present primary user. The projection process is iterated for all angles. Finally, the $\underline{P}$ curve is plotted where primary user(s) have peaks values at their DOAs.

3.1.3 Model Parameters.

This section presents the parameters used to implement the procedure shown in Figure 3.2. The parameters are varied in MATLAB® and are manipulated by the user. Full names and symbolic names of these parameters are given in Table 3.1.

Table 3.1: Single frequency MUSIC algorithm parameters.

Serial	Parameter Name	Symbolic Name
1	Number of sensors	M
2	Number of pimary users	D
3	Signal power per user	S_{pow}
4	Carrier frequency	F_c
5	Total number of collected samples	N
6	Number of streaming bits	$NBits$
7	AWGN standard deviation	σ_n
8	Incident angles vector	$\underline{\theta}$
9	Distance between sensors	d
10	Number of sampled steering vectors $\underline{v}$	pt

3.2 MUSIC for FHSS Signals

This section describes the steps taken to simulate the extended MUSIC algorithm in MATLAB® for FHSS signals. First, the system layout overview and flow chart are shown. Then a table of parameters is provided.

3.2.1 System Layout.

Figure 3.3 shows the general scenario when FHSS signals are present. There are D users transmitting and hopping between a pre-defined set of frequency channels or *hop set*. The operating frequencies are controlled by a pseudo random hopping pattern-generated by LFSR operation. The incident signals hit an array with M sensors. Sensors are equally spaced by distance d. Similar to the previous case defined in section 3.1, the research does not consider the ambiguous cases mentioned in [18]. All incident angles are sampled above Nyquist rate. Each sensor receives total of N sample points during a communication session. The received data at all sesnors' locations are processed and forwarded to an

extended MUSIC block. The next section illustrates the steps taken to determine DOA of FHSS signals utilizing the new development.

3.2.2 Extended MUSIC Process Description.

Figure 3.4 shows the procedure followed to determine DOA of FHSS signals. This procedure represents the extended MUSIC algorithm to determine DOA of FHSS signals.

First, number of sources can be one or more. In this research, all sources are stationary which can represent a geosynchronous satellite. The M sensors receive a delayed copy of the incident signal(s) with respect to a reference sensor. The received vector at the i^{th} sensor operating at frequency bin f_n is given by:

$$\underline{X}_i^n = \underline{a}_i(\theta, f_n)\underline{S}_i^n + \underline{W}. \tag{3.3}$$

where:

$\underline{X}_i^n \in \mathbb{C}^{1\times N_s}$ is the received vector at the i^{th} sensor operating at frequency bin f_n.

$\underline{S}_i^n \in \mathbb{R}^{1\times N_s}$ is the transmitted vector at the i^{th} sensor operating at frequency bin f_n.

$\underline{a}_i(\theta, f_n) \in \mathbb{C}^{1\times D}$ is the steering vector at f_n.

$\underline{W} \in \mathbb{C}^{1\times N}$ is the AWGN.

Then, the matrix for all M sensors at frequency f_n is given by:

$$\begin{bmatrix} \underline{X}_1^n \\ \vdots \\ \underline{X}_M^n \end{bmatrix} = \begin{bmatrix} \underline{a}(\theta_1) & \cdots & \underline{a}(\theta_K) \end{bmatrix} \begin{bmatrix} \underline{S}_1^n \\ \vdots \\ \underline{S}_K^n \end{bmatrix} + \begin{bmatrix} \underline{W}_1^n \\ \vdots \\ \underline{W}_M^n \end{bmatrix}. \tag{3.4}$$

or

$$\mathbf{X}_n = \mathbf{A}_n\mathbf{S}_n + \mathbf{W}. \tag{3.5}$$

where:

$\mathbf{X}_n \in \mathbb{C}^{M\times N_s}$ is the received matrix operating at frequency bin f_n.

$\mathbf{S}_n \in \mathbb{R}^{D\times N_s}$ transmitted matrix operating at frequency bin f_n.

$\mathbf{A}_n \in \mathbb{C}^{M\times D}$ is the array steering matrix.

$\mathbf{W} \in \mathbb{C}^{M\times N_s}$ is the AWGN.

Hence, the net matrix $\mathbf{X} \in \mathbb{C}^{M\times N}$:

$$\mathbf{X} = [\mathbf{X}_1, \cdots, \mathbf{X}_n]. \tag{3.6}$$

Then, the set of eigenvectors associated with the noise subspace when operating at frequency bin f_n is computed in MATLAB®. The previous step is iterated for all frequency bins $\{f_1, f_2, \cdots, f_n\}$. The resulting matrixes are $\{\mathbf{U}_1, \mathbf{U}_2, \cdots, \mathbf{U}_n\}$. Next, a steering vector $\underline{v}(\theta, f_n)$ is picked and projected on the set $\mathbf{U}_1, \mathbf{U}_2, \cdots, \mathbf{U}_n$. The projection coefficients are squared separately and summed:

$$P^{-1}(\theta) = \underline{v}(\theta, f_1)\mathbf{U}_1\mathbf{U}_1^H\underline{v}^H(\theta, f_1) + \underline{v}(\theta, f_2)\mathbf{U}_2\mathbf{U}_2^H\underline{v}^H(\theta, f_2) + \cdots + \underline{v}(\theta, f_n)\mathbf{U}_n\mathbf{U}_n^H\underline{v}^H(\theta, f_n). \tag{3.7}$$

where:

$\mathbf{U}_n \in \mathbb{C}^{M\times M-D}$ is the set of eignvectors associated with the noise subspace operating at frequency bin f_n.

$\underline{v}(\theta, f_n) \in \mathbb{C}^{1\times M}$ is the steering vector at θ and f_n.

The vector $\underline{P}$ is computed and plotted. Peaks of $\underline{P}$ illustrate DOA of a present primary user(s).

3.2.3 Model Parameters.

This section presents the parameters used to implement the procedure shown in Figure 3.4. The parameters are varied in MATLAB® and are manipulated by the user. Full names and symbolic names of these parameters are given in Table 3.2.

3.3 Assessment Methods

This section illustrates the assessment methods to generally evaluate the performance of DOA algorithms. The common assessment methods include beam power side lobes, look angle width and estimate resolution [11]. Other estimation theory related measures

Table 3.2: FHSS MUSIC algorithm parameters.

Serial	Parameter Name	Symbolic Name
1	Number of sensors	M
2	Number of pimary users	D
3	Signal Power per user	S_{pow}
4	Center frequency	F_c
5	Number of samples per frequency hop	N_s
6	Hop set	H_s
7	Number of chips in symbol period	N_c
8	Total number of samples	N
9	Number of streaming bits	$NBits$
10	AWGN standard deviation	σ_n
11	Incident angles vector	$\underline{\theta}$
12	Distance between sensors	d
13	Number of sampled steering vectors $\underline{v}$	pt

include bias and variance of $\hat{\theta}$ [14]. In this research the extended MUSIC algorithm is compared to the conventional MUSIC algorithm. Both algorithms are applied to FHSS signals.

3.3.1 Beam power side lobes.

One way of evaluating performance of DOA is looking at the side lobes of the beam power. Lower side lobes means better performance, less ambiguity and resilience to interference [11]. Researchers have looked at DOA algorithms' performance for correlated and uncorrelated incident signals. Some algorithms have lower side lobes when incidents angles are correlated. However, others such as minimum variance distortionless reposnse

(MVDR) and MUSIC algorithms perform well for both correlated and uncorrelated signals [3, 4, 11].

3.3.2 Look Angle Width.

Width of the look angle is a qualifier of a given DOA estimate. Narrow look angle width and steep beam power value represent a good performance. When the width gets bloated, the outcome starts to be ambiguous. In general, width inflates for low SNR values. Figure 3.5 shows the inflation effect with varying SNR values.

3.3.3 Resolution.

High resolution is one of the attractive features of MUSIC algorithm [15]. High resolution algorithms can identify DOA when source separation decreases in other words, when incident angles values are close. In most cases, resolution increases with increasing number of sensors and vice versa.

3.3.4 Estimator Variance and Bias.

In classic estimation theory, estimators are compared against two measures: bias and variance [14]. The bias of an estimator is the difference between the estimator's expected value and the true value of the parameter being estimated. An estimator or decision rule with zero bias is called *unbiased*. Otherwise the estimator is said to be biased. Unbiased estimators are preferred to biased estimators. The bias of an estimate $\hat{\theta}$ is given by:

$$Bias[\hat{\theta}] = \mathbf{E}[\hat{\theta}] - \theta.$$

The variance of an estimator indicates how far, on average, the collection of estimates is from the expected value of the estimates. High variance illustrates dispersed estimates and hence is unfavorable. Estimate variance is given by:

$$Var[\hat{\theta}] = \mathbf{E}[(\hat{\theta} - \mathbf{E}[\hat{\theta}])^{\mathbf{2}}].$$

An estimate is required to adhere to both properties: being unbiased and having low variance [14]. Figure 3.6 illustrates the bias and variance properties.

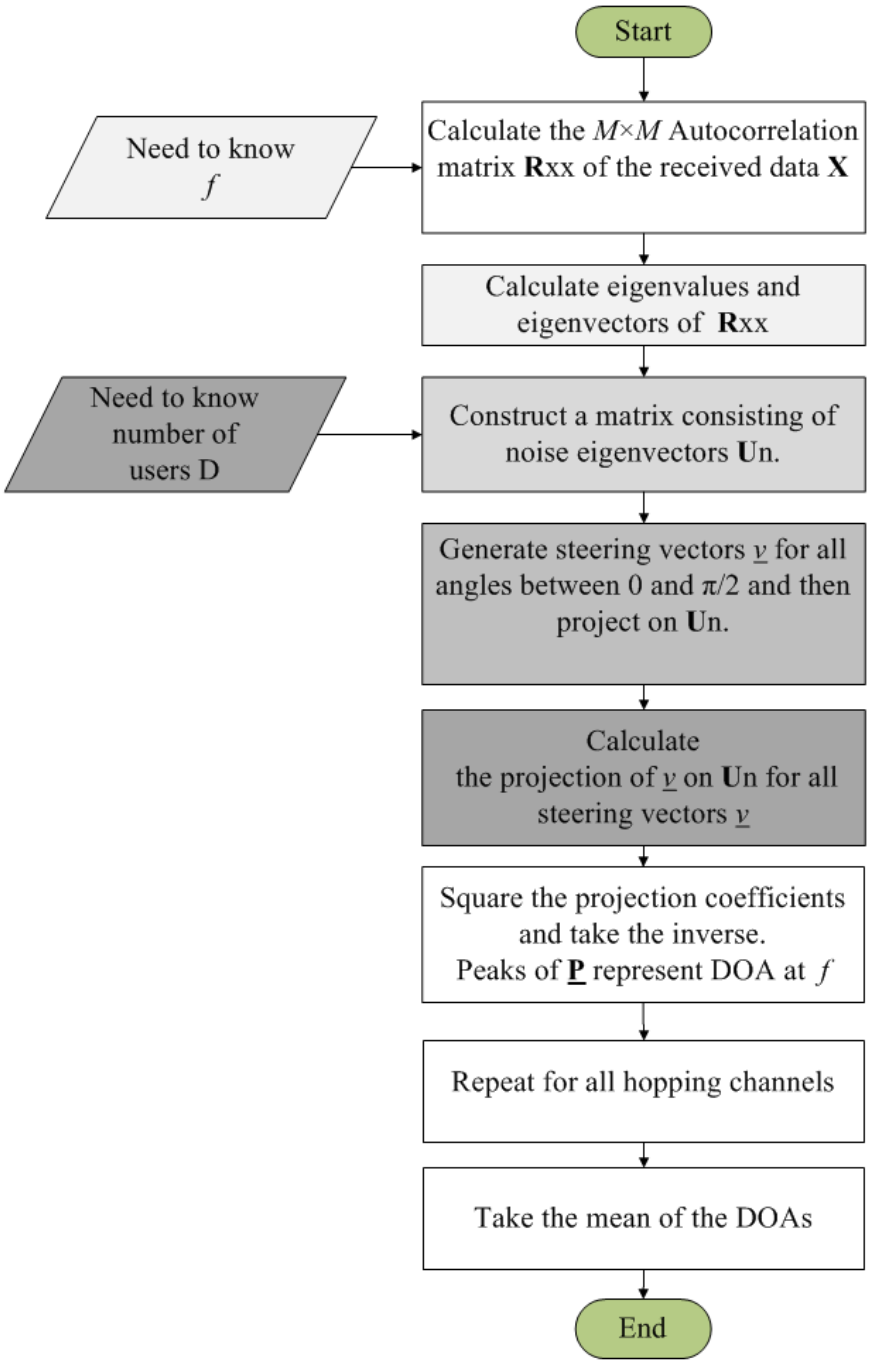

Figure 3.2: Single carrier signals MUSIC flow chart.

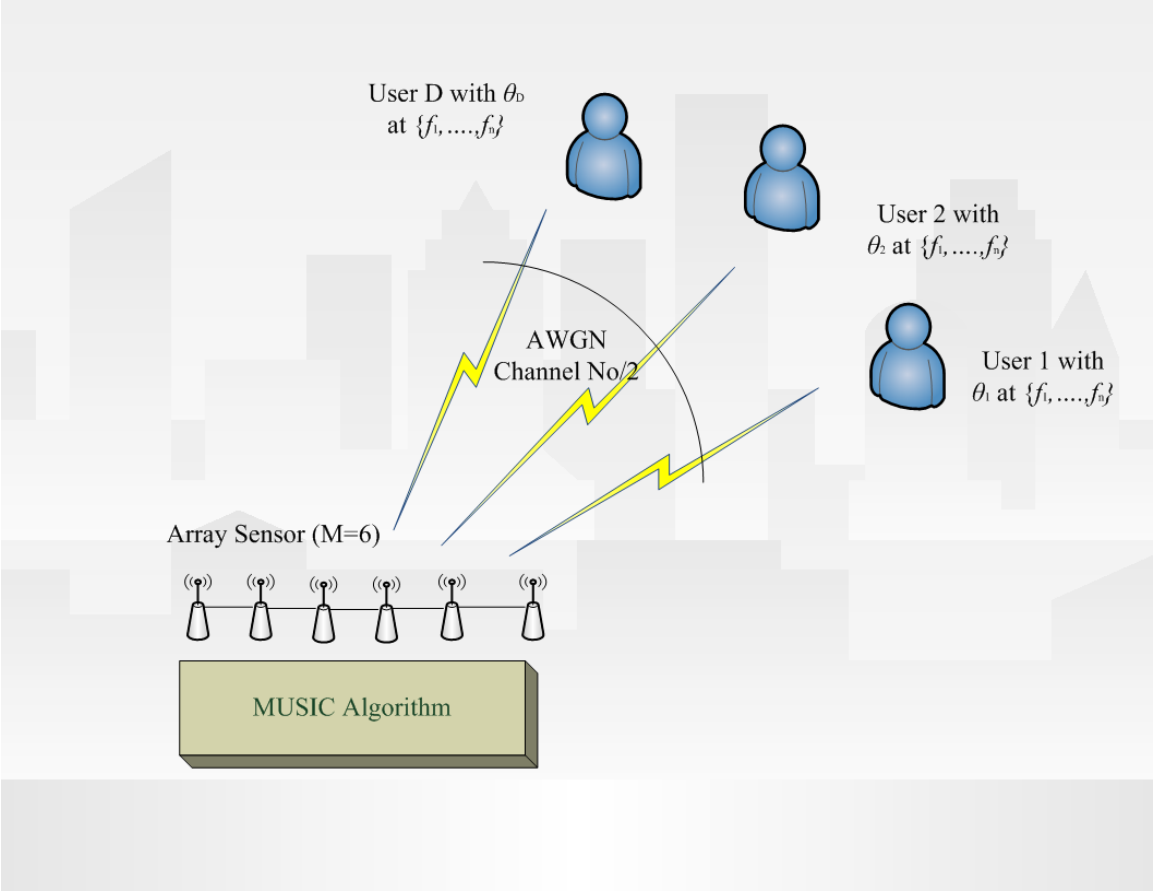

Figure 3.3: FHSS algorithm DOA problem.

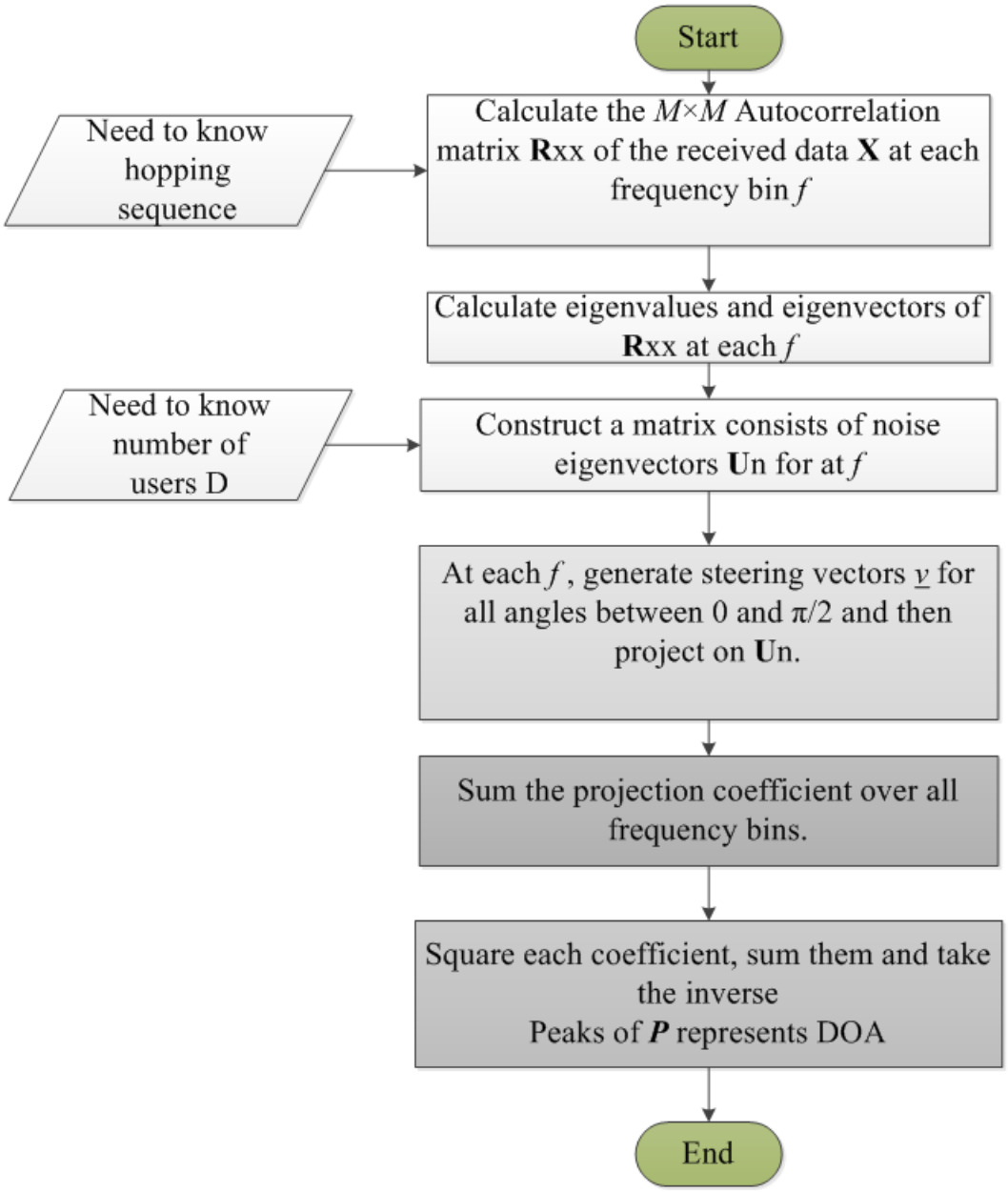

Figure 3.4: FHSS MUSIC algorithm flow chart.

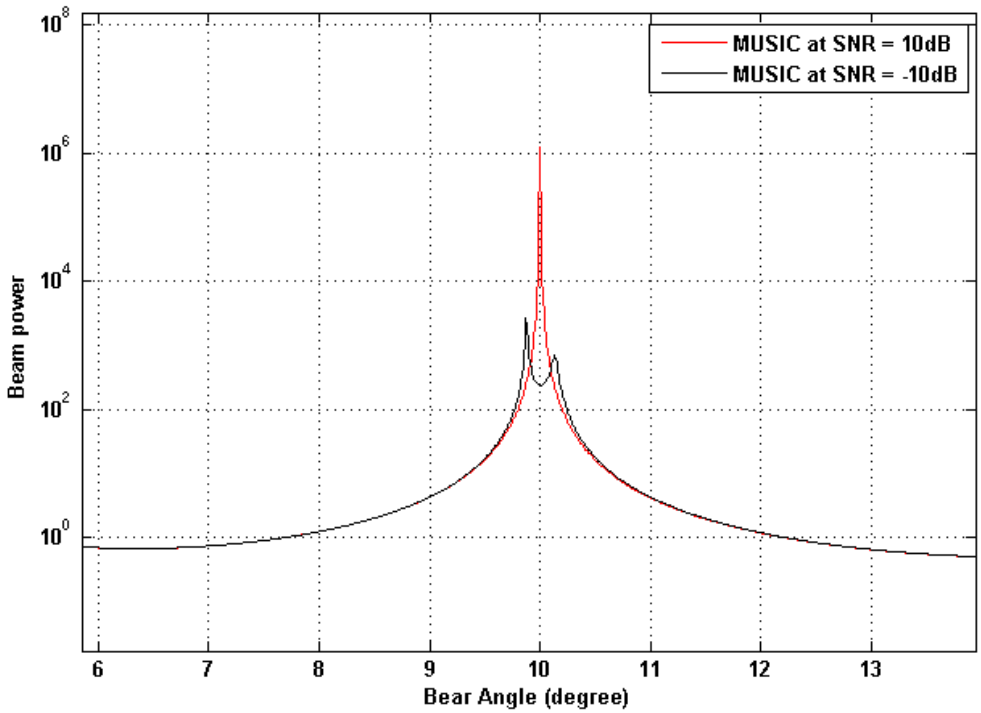

Figure 3.5: MUSIC at different SNR levels.

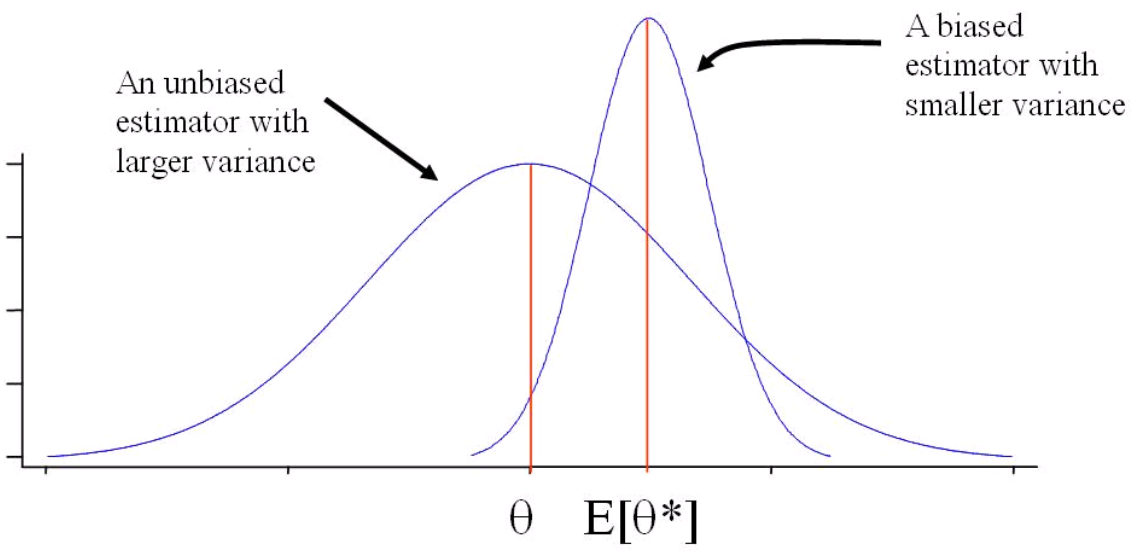

Figure 3.6: Illustrative bias and variance properties.

IV. Simulation Results and Analysis

This chapter describes the simulation setup, results and analysis of the single frequency MUSIC algorithm and FHSS algorithm to determine DOA of FHSS signals. First, the simulation setup is explained including the parameter values used to produce the results in this thesis. Then, the results of the qualifiers used to assess the performance of both processes are given. Finally, the analysis for the synchronization time of FHSS systems is discussed.

4.1 Simulation Setup

The DOA estimation using MUSIC algorithm is tested for single frequency algorithm and FHSS algorithm. The comparison is carried for different SNR levels, number of samples N_s, number of sensors M and number of hops H_s. The simulation process is thoroughly explained in Chapter III. However, in this section, actual simulated parameter values are given to produce the results shown later in this chapter. Table 4.1 shows the parameter values assigned to simulate single frequency MUSIC algorithm. This step comprises baseline data to compare it with the new development later. The SNR, N_s, M and H_s values are varied to assess different effects and dimensions. Signal power, array sensor locations, number of bits and carrier frequency F_c are kept constant in this simulation. The ultimate goal is to perform sensitivity analysis of the qualifiers mentioned above and hence a fair decision could be made.

Table 4.2 shows the parameter values used to produce the results of FHSS MUSIC algorithm. The given values are the unchanged ones carried in the sensitivity analysis of both systems.

Table 4.1: Single frequency MUSIC algorithm simulation parameters.

Serial	Parameter Name	Symbolic Name	Value
1	Signal power per user	S_{pow}	$1W$
2	Carrier frequency	F_c	10 kHz
3	Number of streaming bits	$NBits$	600 bits
4	Distance between sensors	d	$\frac{\lambda}{2}$
5	Number of sampled steering vectors $\underline{v}$	pt	1000
6	Monte Carlo trials	$Monte$	10000
7	Symbol duration	T_{Sym}	0.01 sec

4.2 Assessment Results

MUSIC algorithm is performed for the single frequency algorithm and the new development to determine DOA of the FHSS signals. The thesis emphasizes that the new development outperforms the conventional method. This section gives the results of varying SNR value, number of samples N_s, number of sensors M and hop set value H_s. These parameters measure the performance of both methods. The results are discussed and analyzed.

4.2.1 SNR Level.

The simulation was first carried out for the single frequency algorithm to estimate DOA of FHSS signals. The parameter values are given in Table 4.3. The SNR value was swapped between various values to simulate different noise levels. The other examined parameters are kept to standard values throughout this experiment. An estimate of the average DOA is calculated for every SNR value. After that, the new development is

Table 4.2: FHSS algorithm simulation parameters.

Serial	Parameter Name	Symbolic Name	Value
1	Signal power per user	S_{pow}	$1W$
2	Carrier frequency	F_c	10 kHz
3	Number of streaming bits	$NBits$	600 bits
4	Distance between sensors	d	$\frac{\lambda}{2}$
5	Number of sampled steering vectors $\underline{v}$	pt	1000
6	Monte Carlo trials	$Monte$	10000
7	Symbol duration	T_{Sym}	0.01 sec
8	Chip duration	T_c	0.1 sec
9	Number of bits in chip	N_c	10 bits

executed to determine DOA of FHSS signals. Similarly, the SNR values are changed every time to simulate different SNR points. It should be mentioned that the noise realization for a given SNR level is the same for both systems meaning that they experienced the same noise effect.

As mentioned in Chapter III, there is a two-dimensional evaluation measure for a classical estimation problem: *bias* and *variance*. The bias of the DOA estimate is calculated for both systems. Figure 4.1 illustrates the bias for different SNR levels.

At very low SNR values, the single carrier frequency system shows arbitrary large bias on its way to a regular descent as SNR value increases. The FHSS system, on the other

Table 4.3: SNR simulation parameters.

Serial	Parameter Name	Symbolic Name	Value
1	Signal to noise ratio	SNR	$\{-10, -9, \cdots, 20\}$ dB
2	Number of hops	H_s	8
3	Samples at a frequency bin	N_s	2500
4	Number of sensors	M	13
5	Single carrier bandwidth	W_{single}	200 Hz
6	FHSS bandwidth	W_{FHSS}	900 Hz
7	Number of users	D	1
8	Incident angle	θ	40°

hand, starts low and consistent for all SNR values. The FHSS system bias decreases as SNR increases. Both systems have a low bias at high SNR values.

The variance of the DOA estimate is calculated for both methods. The variance is calculated by running a given system for a specific SNR value for 10000 Monte Carlo trials. The standard deviation is computed by taking the square root of the variance. Figure 4.2 shows the variances of both estimators.

At low SNR values, the FHSS system has a moderate value then drops to lower values at high SNR values. The single frequency system starts at a high level and drops to lower values at high SNR values. The overall standard deviation of the FHSS system is lower compared to the single frequency system.

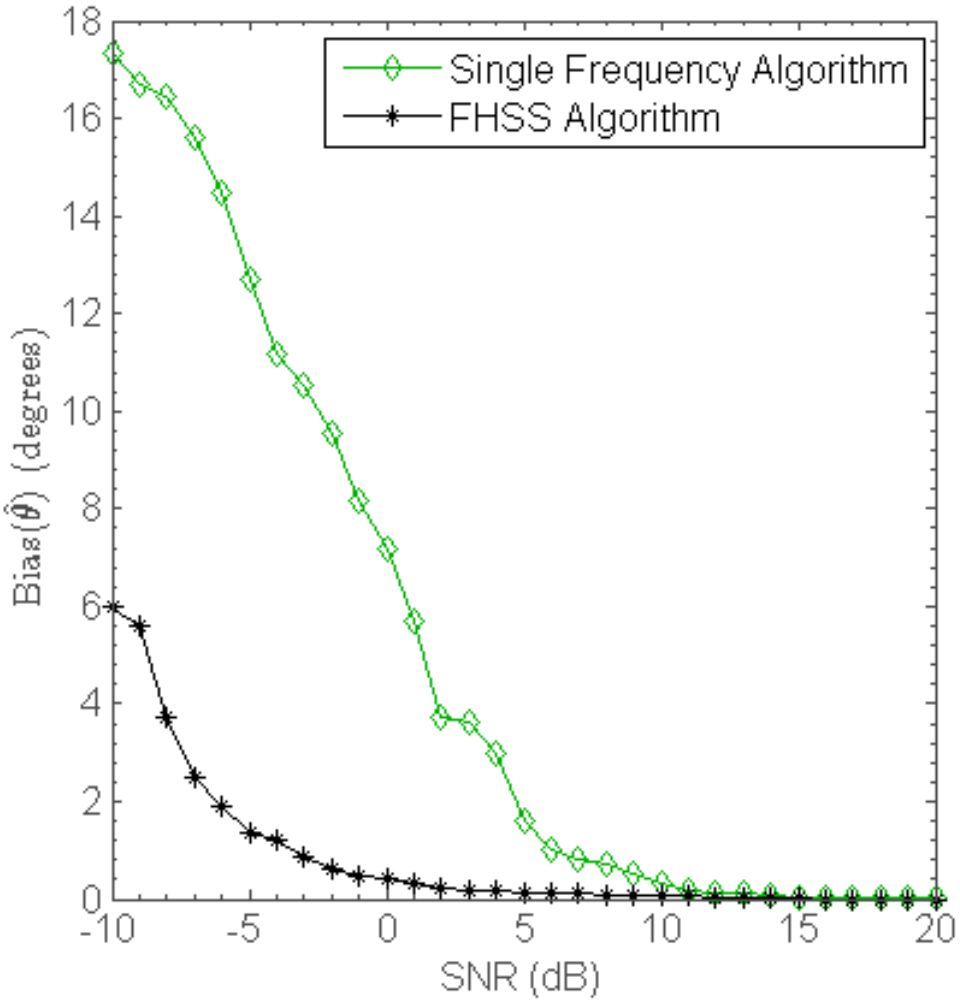

Figure 4.1: DOA estimation bias vs. SNR.

Another important qualifier mentioned in Chapter III is level of side lobes variance or standard deviation $\sigma_{sidelobe}$. It is defined as the variance of the beam power outside the look angle portion which is about 13°. The lower the value, the better performance is. Figure 4.3 shows the average standard deviation of the side lobes of both systems for various SNR values.

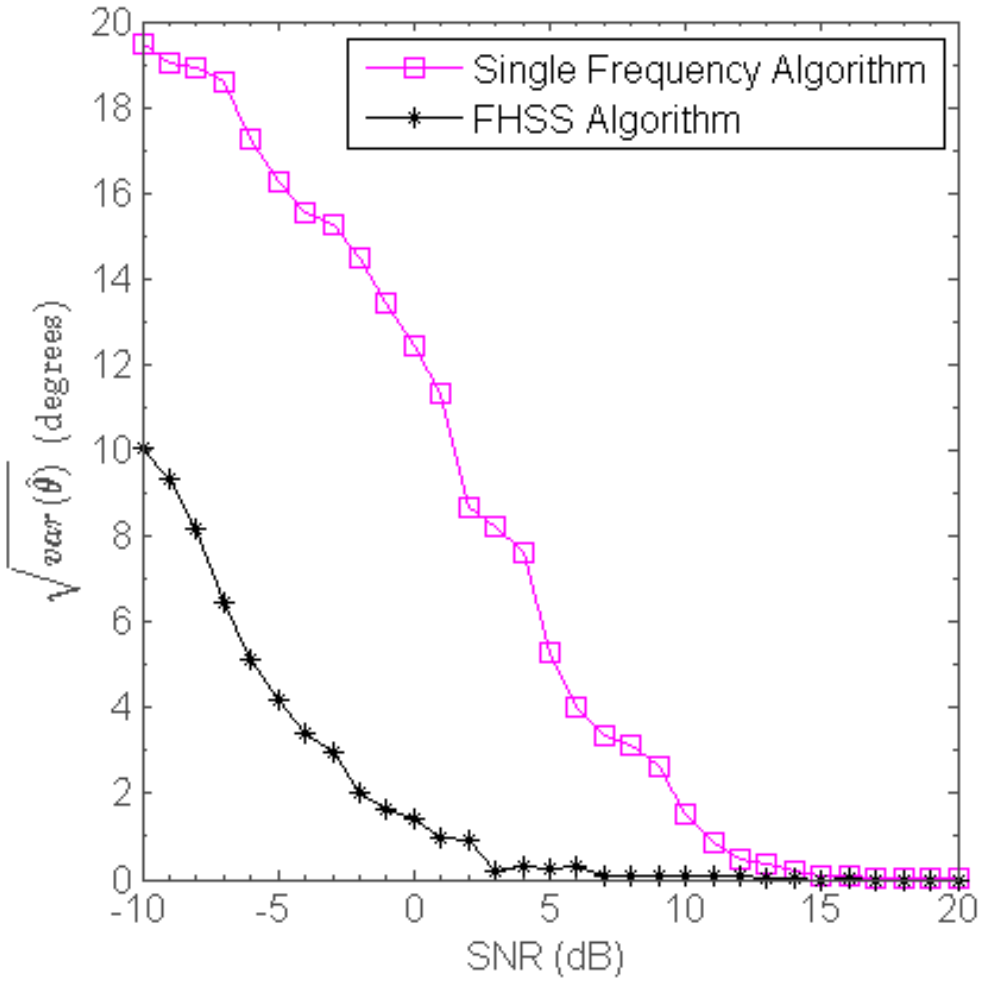

Figure 4.2: DOA estimate standard deviation vs. SNR.

The standard deviation of the single frequency system starts very high at low SNR values. Conversely, the FHSS system shows a low side lobe standard deviation compared to the single frequency system and then takes its way to lower values as SNR increases. It should be mentioned that the single frequency system can result in ambiguous values due to high side lobe variance. High side lobe variance can relate to the large bias shown for the single frequency system since the receiver has no way of identifying the true incident angle(s).

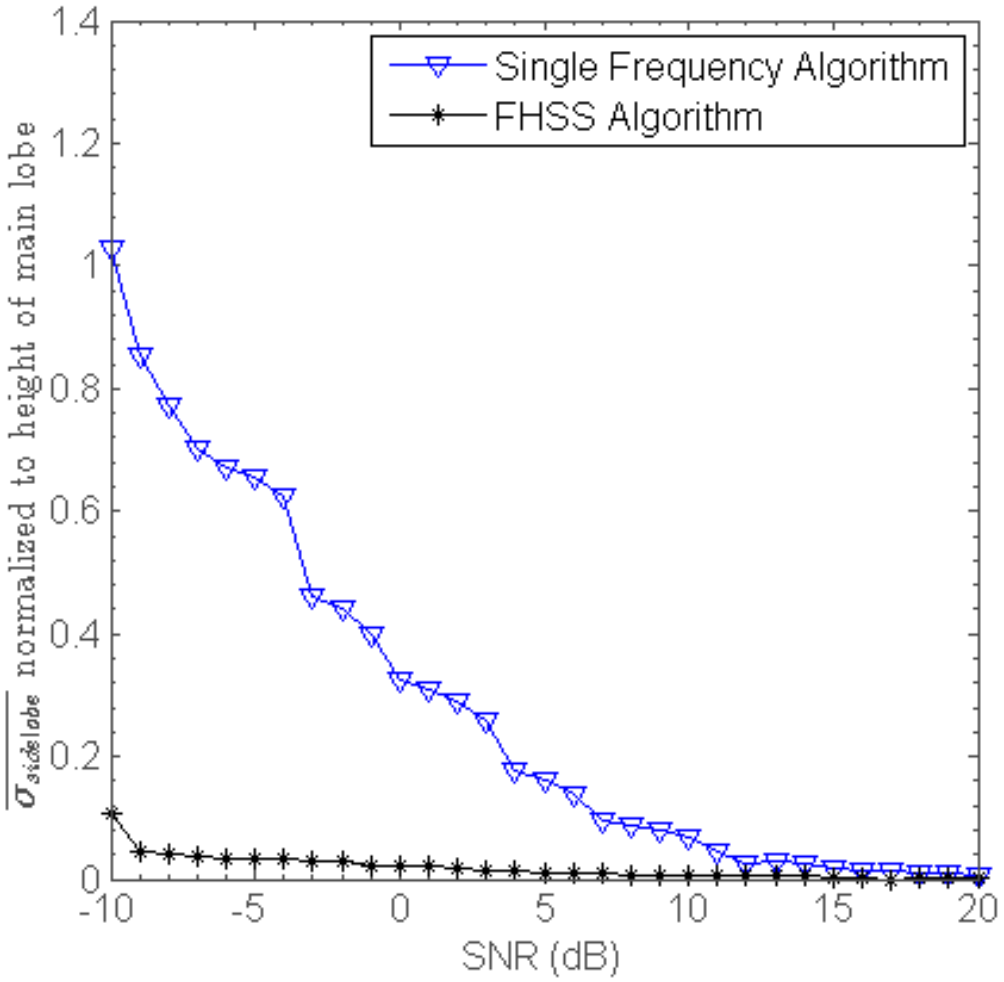

Figure 4.3: Average side lobes standard deviation.

4.2.2 Number of Samples N_s.

Number of samples N_s taken at a given frequency bin was one of the measures used to evaluate system performance. As N_s increases, the magnitude of the beam power or response increases. Hence, the receiver would have higher probability of detecting the true incident angle(s) for larger values of N_s. In this portion of the simulation, the N_s values were swapped while other examined parameters were fixed. The goal of this step was to study the effect of changing N_s value for both systems while keeping standard values for

the other set of parameters examined in this simulation. Table 4.4 shows the parameter values assigned in this section of the simulation.

Table 4.4: Simulation parameters when N_s varies.

Serial	Parameter Name	Symbolic Name	Value
1	Signal to noise ratio	SNR	0 dB
2	Number of hops	H_s	8
3	Samples at a frequency bin	N_s	$\{2500, 3000, 3500, \cdots, 10000\}$
4	Number of sensors	M	13
5	Single carrier bandwidth	W_{single}	200 Hz
6	FHSS bandwidth	W_{FHSS}	900 Hz
7	Number of users	D	1
8	Incident angle	θ	40°

The noise effect in this experiment is fixed and the number of samples N_s was changed. The minimum N_s value that could be used in this experiment and yet avoid aliasing effect is given by Equation (4.1). The N_s value started at 2500, a bit higher than the lower bound (2020 samples), to 10000 collected points at every frequency bin.

$$min_{pt} = \frac{2(F_c + W/2)T_{Sym}}{N_c}. \tag{4.1}$$

where:

F_c is the carrier frequency in Hz.

W is the null to null bandwidth in Hz.

T_{Sym} is the symbol duration in *sec*.

N_c is the chip duration in *sec*.

The simulation was first carried for the single carrier frequency system for various N_s values. At a given N_s value, the conventional MUSIC is executed for 10000 Monte Carlo trials. At each trial, an estimate is computed and at the end of the trials, an average estimate is recorded. The mean estimate is compared to the true value and the bias at this N_s value is saved. Next, utilizing the 10000 trials performed at every simulated point, a variance of the estimate could be calculated for different N_s values.

Similarly, the FHSS system was run for different N_s values experiencing the same noise effect encountered by the single frequency system. The N_s values were changed to obtain different simulation points. At a given N_s value, the extended MUSIC system is applied for 10000 Monte Carlo trials. Bias and variance of this estimate were calculated and saved for all N_s values. Figure 4.4 and Figure 4.5 show the bias and variance for both systems, respectively.

According to Figure 4.4, the overall single frequency system bias is relatively high compared to FHSS system. The bias decreases as N_s value increases. On the other hand, the FHSS system starts with a low bias at low N_s values and consistently takes the way to low and steady bias as N_s value increases.

Figure 4.5 shows the standard deviation of the estimate for the two systems. The single frequency system estimate standard deviation starts high and random for low N_s values. Then, the curve descends to a moderate value as N_s value increases. On the other hand, The FHSS system has low standard deviation at low N_s values and decreases further as N_s value increases. The FHSS system reaches a steady-state point where no further improvement can be achieved.

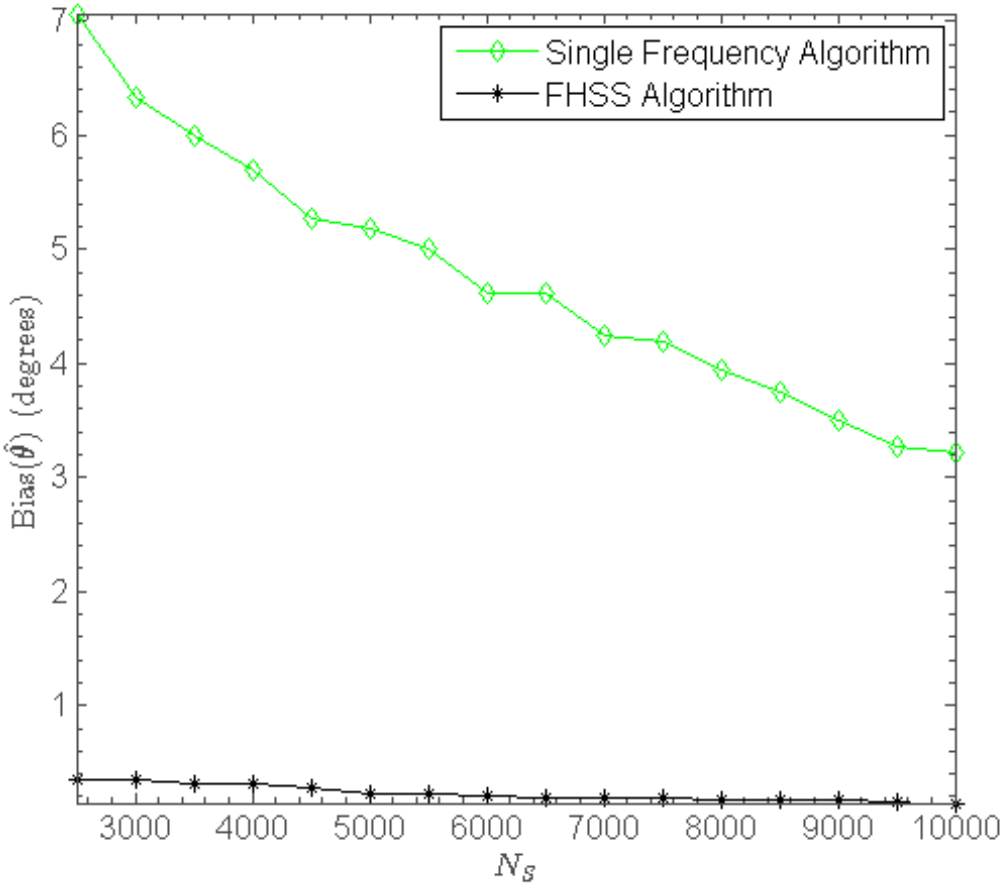

Figure 4.4: Bias vs. N_s.

4.2.3 Number of Hops H_s.

This section of the simulation process captures the effect of expanding the hop set value and the consequences it may have on the DOA estimation. The H_s value was varied to study the effect on the FHSS system and compare it to the single frequency system. The other examined parameters were fixed. Table 4.5 shows the values used in this part of the simulation.

Changing the H_s value affects the occupied bandwidth. Increasing number of hops results in larger bandwidth. The null-to-null bandwidth and H_s relationship is illustrated

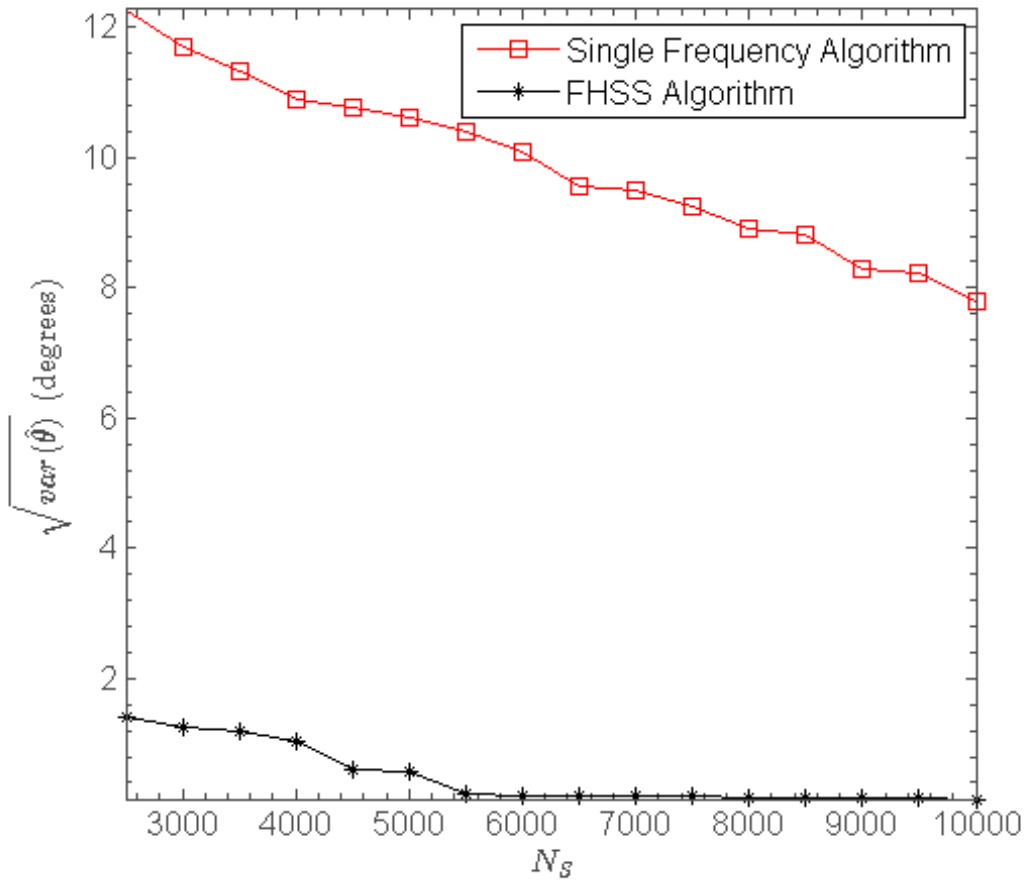

Figure 4.5: Standard deviation vs. N_s.

by Equation (4.2).

$$W_{FHSS} = \frac{H_s + 1}{T_{Sym}}. \tag{4.2}$$

where:

W_{FHSS} is the FHSS bandwidth in Hz.

H_s is the number of hops.

T_{Sym} is the symbol duration in *sec*.

In Chapter II, the theory of the MUSIC algorithm exploits the orthogonality property between the signal subspace and the noise subspace of the covariance matrix. It is known

Table 4.5: Simulation parameters when H_s varies.

Serial	Parameter Name	Symbolic Name	Value
1	Signal to noise ratio	SNR	0 dB
2	Number of hops	H_s	$\{1, 4, 8, 16, 32\}$
3	Samples at a frequency bin	N_s	2500
4	Number of sensors	M	13
5	Single carrier bandwidth	W_{single}	200 Hz
6	FHSS bandwidth	W_{FHSS}	$\{200, 500, 900,$ $1700, 3300\}$ Hz
7	Number of users	D	1
8	Incident angle	θ	40°

that the signal subspace is a function of the carrier frequency F_c. Therefore, the FHSS signal has signal subspace with rank equal to H_s value. The overall signal subspace is the union of the individual subspaces. Therefore, the MUSIC algorithm estimation becomes better in the sense of capturing multiple effects of different signal subspaces. The results Figure 4.6 and Figure 4.7 illustrate the performance of the two systems at various H_s values.

The single frequency system has a constant bias and variance for all H_s values. The bias and the standard deviation are relatively high at the standard values shown in Table 4.5.

The FHSS system bias and standard deviation drops to a low value and stays almost steady for all H_s values. The main conclusion is that the FHSS system reaches a steady state point where no further improvment can be achieved.

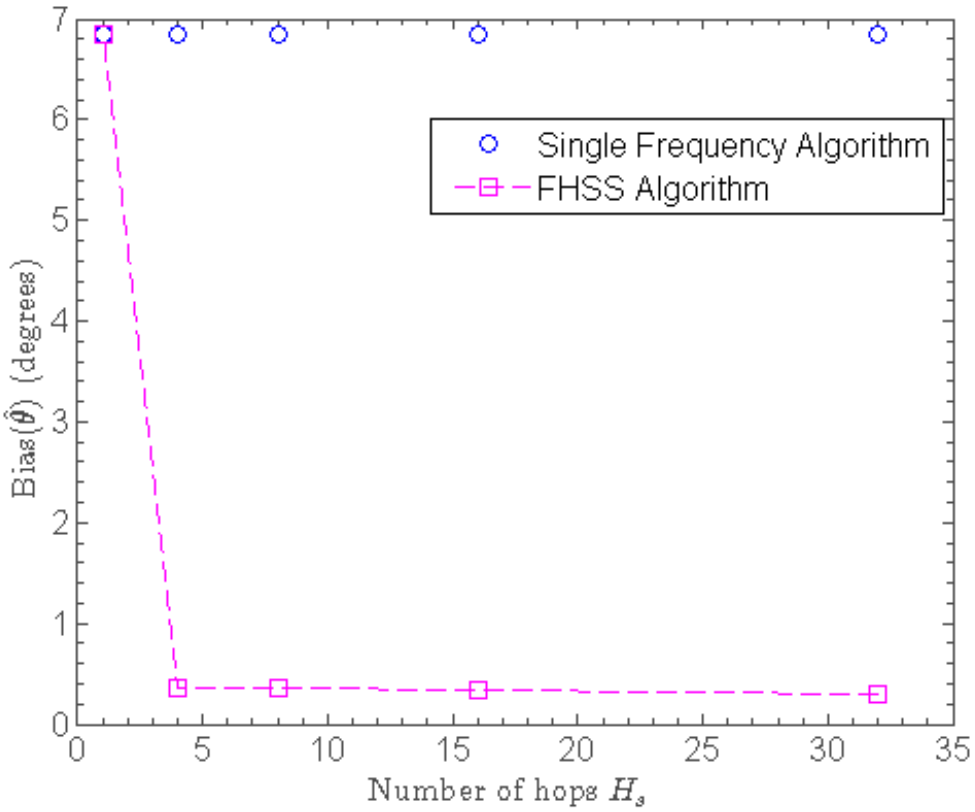

Figure 4.6: Bias vs. H_s.

4.2.4 Number of Sensors M.

The last parameter varied in the simulation part was number of sensors M. All other examined parameters were fixed to study the effect of swapping M. This simulation section started by creating 2 primary users at different incident angles. The single frequency system was executed first and the response was recorded for various M values. Then, the FHSS system was simulated for the same set of M values. Table 4.6 shows the parameter values involved in this experiment.

Figure 4.8 shows the MUSIC beam power curves for the two systems using the set of values shown in Table 4.6. The following comment could be made:

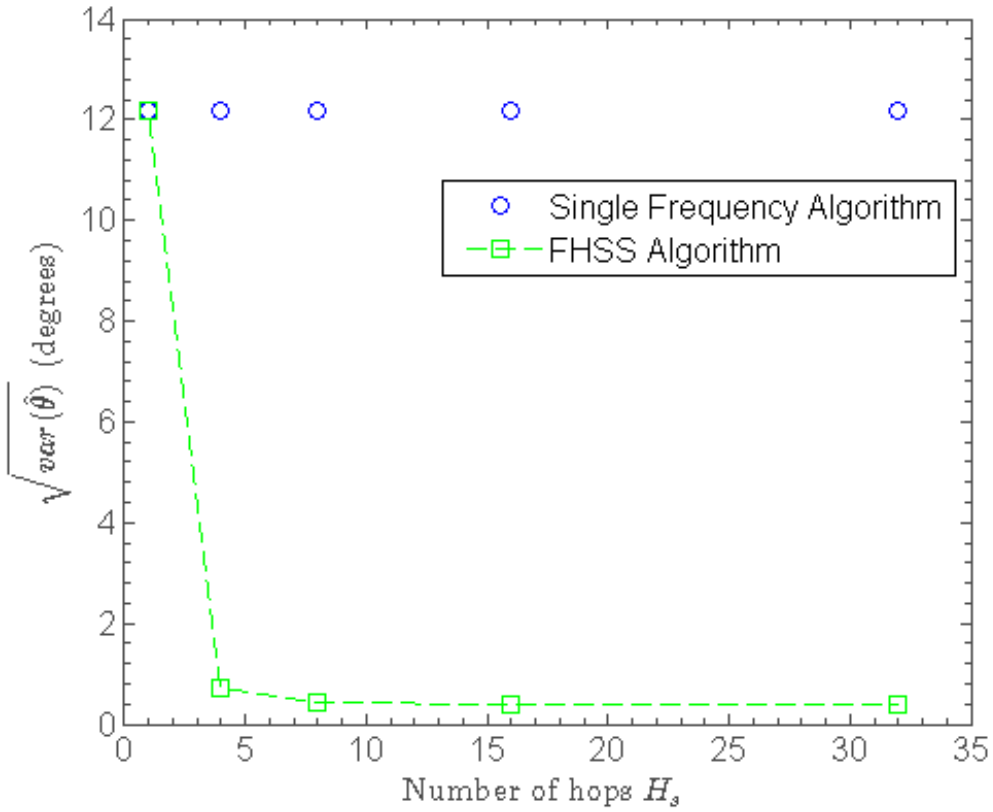

Figure 4.7: Standard deviation vs. H_s.

- The FHSS system has lower beam power values outside the look angle points compared to the single frequency system for all M values. As discussed in Chapter III, the lower the side lobes, the better the performance is.

- Both FHSS system and single frequency system has similar values at the look angle points. When $M = 25$ sensors, the beam power values at the look angle points of the FHSS system is slightly below the other systems values. However, most of the times the FHSS either surpasses or equals to the single frequency system values.

- When M increases, the resolution of the single frequency system increases. However, the FHSS system resolution has a very good resolution even at low number of

Table 4.6: Simulation parameters when M varies.

Serial	Parameter Name	Symbolic Name	Value
1	Signal to noise ratio	SNR	0 dB
2	Number of hops	H_s	8
3	Samples at a frequency bin	N_s	2500
4	Number of sensors	M	$\{10, 13, 15, 20, 25\}$
5	Single carrier bandwidth	W_{single}	200 Hz
6	FHSS bandwidth	W_{FHSS}	900 Hz
7	Number of users	D	2
8	Incident angle	$\underline{\theta}$	$\{40°, 60°\}$

sensors. When $M = 10$, for example, the single frequency system can hardly distinguish between the two users. The FHSS, on the other hand, has two fair peaks at the two incident angles. In comparision, the single frequency system starts to show notable peaks when $M = 25$.

- The single frequency system degrades severely when it comes to the width of the look angles. Actually, the widths are fairly large even for high values of M. Conversely, the FHSS system has pretty steep and narrow beam power values near the look angles. The widths values get narrower when M increases.

4.3 Synchronization Time

Based on the analysis discussed above for different parameter values, the FHSS system by far outperforms the conventional single frequency system. However, there are some drawbacks to this development. The occupied bandwidth was one of the downsides mentioned above. The other downside is called synchronization time. The FHSS system takes some time to get the receiver and the transmitter synchronized. This section studies the synchronization time for the FHSS system when varying H_s value and SNR levels.

4.3.1 Synchronization Time for Various SNR Levels.

The simulation in this experiment is similar to the one discussed in section 5.2.1. The parameter values are the same ones shown in Table 4.3. However, this time, the attention was directed to capture the effect on the synchronization time for various SNR levels.

For a given SNR level, the receiver starts listening at a random frequency channel. Similarly, the transmitter begins transmitting at random frequency channel. The selection of both receiver and transmitter channels are independent. The transmitter broadcasts the synchronization message at the pre-selected frequency channel. If the receiver happens to be on that frequency channel, then the acknowledgement message is sent back to the receiver and the synchronization is achieved. If not, the transmitter hops to another random frequency channel and resends the synchronization message again. The receiver, on the other hand, stays at the same pre-selected frequency channel. This process keeps going until both the transmitter and the receiver meet on a common frequency channel and the acknowledgement is achieved. The time elapsed is recoded until the acknowledgement is confirmed. In this experiment, the synchronization time is expressed in terms of the symbol duration T_c. The previous synchronization process is iterated for various SNR values.

Figure 4.9 shows the synchronization time in terms of symbol duration T_c for different SNR levels. According to the Figure 4.9, two factors can affect the synchronization time: SNR level and the randomness of frequency channel selection. The transmitter may hop to

the receiver channel early but if the noise level is high, the receiver might not recognize the synchronization message and hence misses the turn resulting in a longer synchronization time. The previous case could be reversed. The receiver may exist on the last hop station of the transmitter although the noise level is low. Both cases can happen simultaneously resulting in the most possible synchronization time that can occur. The previous discussion was the main rationale to examine another parameter to get a fair insight into the factors that can affect the synchronization time. Generally, the overall take away of Figure 4.9 is that synchronization time decreases as SNR level increases.

Let **p** be an uniform random variable (RV) such that **p** represents the next hopping channel . Then, **p** can take a value from 1 to 8. Therefore,

$$\mathbf{p} \sim \mathcal{U}(1, 8)\,. \tag{4.3}$$

The average value of the RV(**p**) can be calculated as:

$$\mathbf{E}[\mathbf{p}] = \frac{8-1}{2}. \tag{4.4}$$

$$\mathbf{E}[\mathbf{p}] = 3.5. \tag{4.5}$$

The simulation results shown in Figure 4.9 matches the value calculated above after 10000 trials and when SNR increases.

4.3.2 Synchronization Time for Various H_s Values.

To clear the ambiguity discussed above regarding the overlapping of the SNR level and the H_s value effects, the noise level in this section is kept constant at 0 dB and the H_s value was varied similar to the case discussed in section 5.2.3. The synchronization process was mentioned in section 5.3.2 or Chapter II.

For low H_s values, the transmitter and the receiver are more likely to co-exist on the same frequency channel since there arent too many channels to choose from. On the other hand, if H_s increases, the number of frequency channel choices increases. Consequently,

the probability of the transmitter and the receiver to meet early on a common frequency channel is low.

Figure 4.10 shows the synchronization time in terms of T_c for various values of H_s. The relation is linear and stems from Equation (4.5) except number of hops H_s is variable. Therefore,

$$\mathbf{E}[\mathbf{p}] = \frac{H_s - 1}{2}. \tag{4.6}$$

As H_s increases, the synchronization time increases as well which confirms the discussion above. Conversely, when the number of hops is low the synchronization time is minimal.

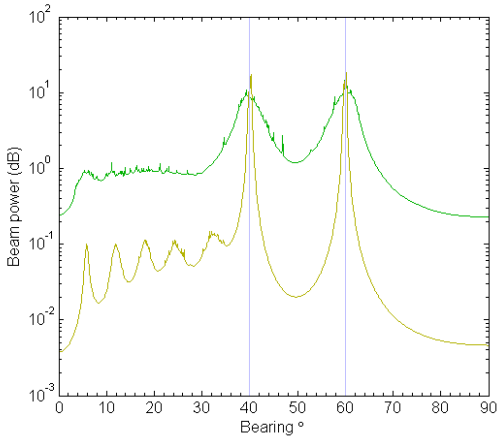

(a) $M = 10$

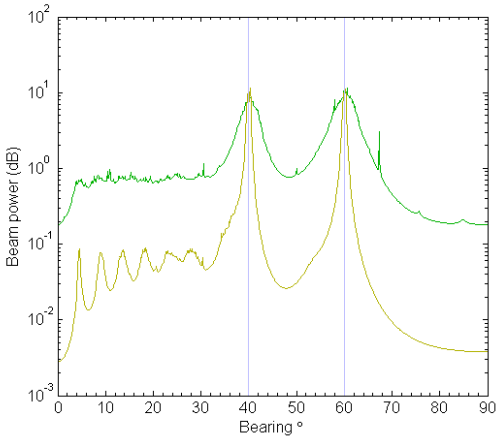

(b) $M = 13$

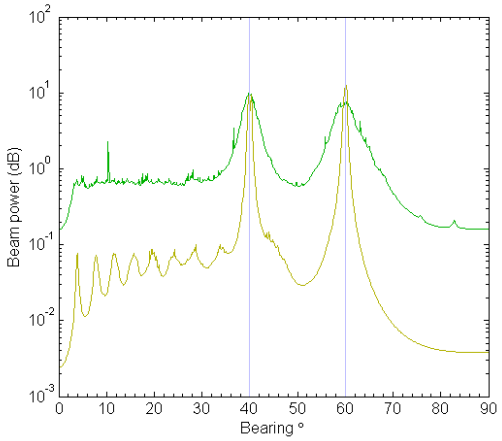

(c) $M = 15$

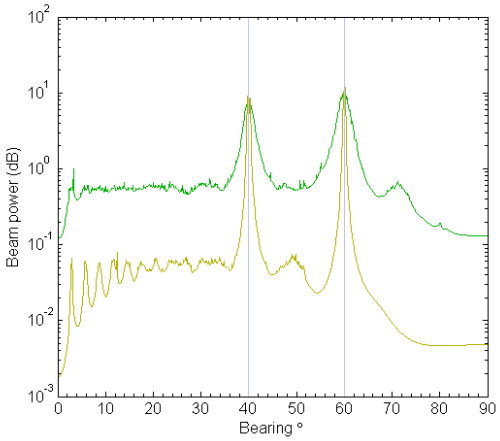

(d) $M = 20$

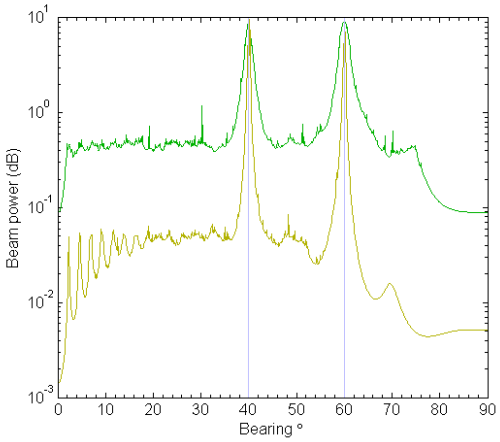

(e) $M = 25$

Figure 4.8: MUSIC DOA estimation of both systems for various M values.

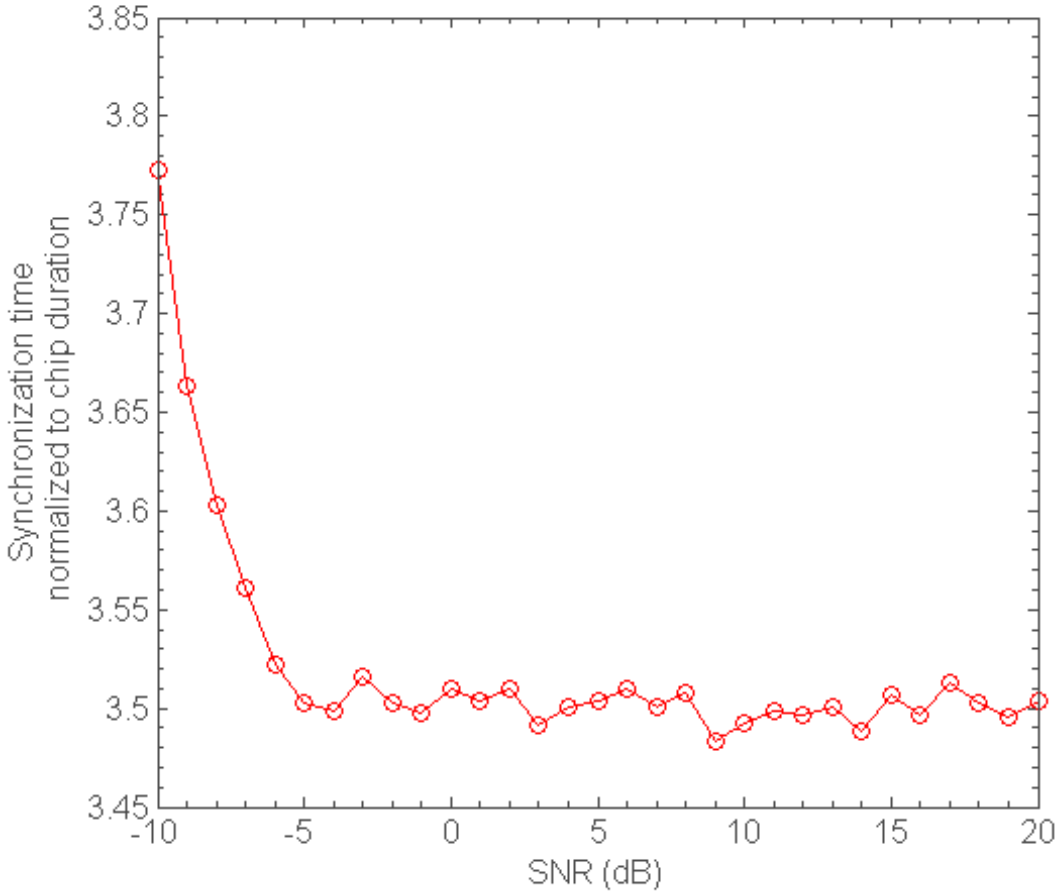

Figure 4.9: Synchronization time of the FHSS system for various SNR values.

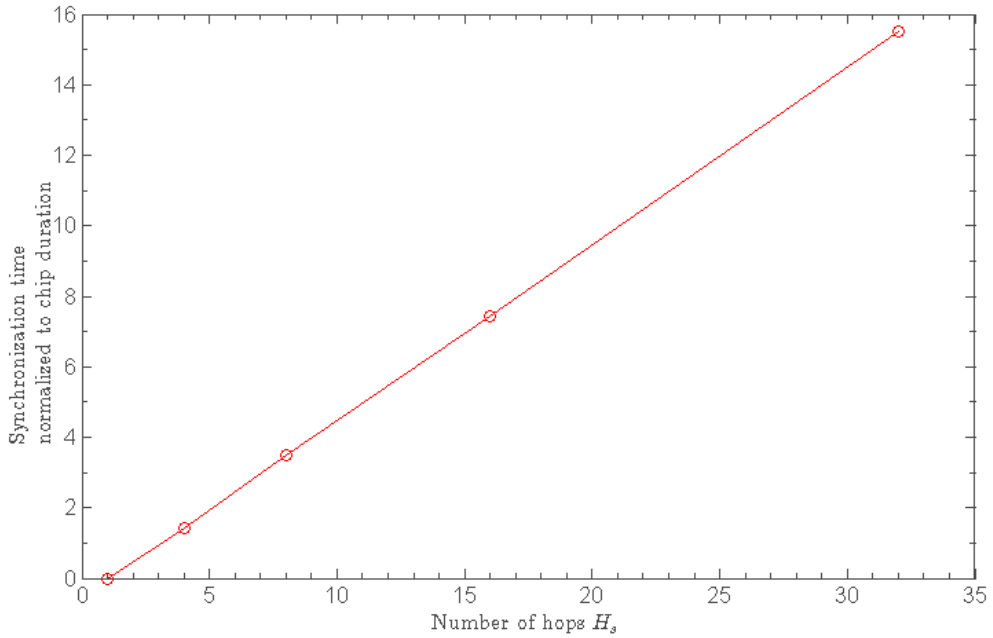

Figure 4.10: Synchronization time for various H_s values.

V. Conclusions

The goal of this thesis was to advance the work on the MUSIC algorithm to estimate DOA of incidents angle(s) of FHSS signals. The existing algorithm works for narrow band single hop signals. The objective was to develop a procedure to execute MUSIC as a one time algorithm for multiple-hop signals and study the performance of the new development. The new system was simulated for varying SNR, N_s , N and H_s values. The bias and variance of the two systems were plotted and discussed.

5.1 Summary

A MUSIC algorithm for DOA estimation was developed for FHSS signals to determine, as accurately as possible, the incident angles of present primary users. First, the FHSS signal generator with its peripherals, such as hopping pattern, were coded in MATLAB®. The generator was tested to ensure it was correctly simulating FHSS signals. Then, the conventional MUSIC algorithm was applied seperately for all frequency channels to estimate DOA of FHSS signals. The SNR level was varied to test the performance in varying noise levels. The bias and variance of the estimate were recorded for later comparison. Number of collected samples was varied as well to look at the bias and variance of the estimate. After that, number of hops H_s was varied. Then, number of sensors N was changed to test the resolution of the existing system.

Then, the new MUSIC algorithm was executed to estimate DOA of the incident angles. The new system was tested under various noise levels. In addition, it was studied for different hop set values. Then, the number of sensors was changed to observe the resolution and resiliency of the new system. Finally, number of collected samples at a frequency bin was swapped. The bias and variance were observed and recorded for all

examined parameters. A thorough discussion and comparison were carried to highlight the differences between the two systems.

5.2 Findings

As mentioned above, both systems were tested under various situations. The followings findings were observed:

- The developed MUSIC algorithm had lower bias and variance compared to the single frequency algorithm for all SNR values. For both systems, estimates the bias and variance decrease when SNR increases.
- When reducing N_s value, the FHSS system outperformed the single frequency algorithm. The bias and variance of both estimates were plotted and studied.
- The resolution of the FHSS system was by far better compared to the single frequency system even for low number of array sensors M. As a matter of fact, the single frequency algorithm resolution needed more sensors to starts distinguishing close incident angles.
- The bias and variance of the new developed FHSS MUSIC algorithm dropped to a steady figure for all H_s values.

Despite the performance improvement of the FHSS system, there are limitations to address:

- Number of primary users K was known in this development.
- To be able to execute the new development, one should know the hopping pattern of the FHSS signals.
- Synchronization time is an issue when it comes to robustness of the system. The FHSS system needs time to synchronize which was not the case for the single carrier system. The synchronization time was discussed and studied for various noise levels and hop set values.

5.3 Impact

This research has taken the most popular signal subspace approach DOA algorithm to estimate the incident angles of FHSS signals. FHSS signals are widely used in military applications to mitigate possible jamming attacks. The need for a high resolution DOA algorithm to determine incident angles of FHSS signals is growing. This research has touched this area and shows that the MUSIC algorithm can be extended to this type of signals. Results were discussed, explained and compared to the existing development.

5.4 Recommendation for Future Work

The MUSIC algorithm is a challenging area and popular for DOA estimation. At the same time, the need for wide band signals, such as FHSS, DOA estimation is growing. Researchers have looked at wide-band signals DOA estimation in a general manner. However, there are some obstacles and limitations for those approaches. This thesis has taken the conventional and robust basic MUSIC algorithm and expanded it for FHSS signals with the least complexity and latency. This work can be advanced by looking at number of signals estimation and hopping pattern estimation. By doing so, a complete, robust and high resolution MUSIC algorithm for FHSS signals can be obtained.

Bibliography

[1] Alghamdi, O.A. and M.A. Abu-Rgheff. "Performance evaluation of cognitive radio spectrum sensing using multitaper-singular value decomposition". *4th International Conference on Cognitive Radio Oriented Wireless Networks and Communications*, 1–6. 2009.

[2] Axell, E., G. Leus, E. G. Larsson, and H. V. Poor. "Spectrum Sensing for Cognitive Radio : State-of-the-Art and Recent Advances". *IEEE Signal Processing Magazine*, 29(3):101 –116, May 2012.

[3] Balabadrapatruni, Sai Suhas. "Performance Evaluation of Direction of Arrival Estimation Using MATLAB". URL http://arxiv.org/pdf/1211.4442.pdf.

[4] Benesty, J., Jingdong Chen, and Y.A. Huang. "A generalized MVDR spectrum". *IEEE Signal Processing Letters*, 12(12):827–830, 2005.

[5] Bienvenu, G. "Eigensystem properties of the sampled space correlation matrix". *IEEE International Conference on Acoustics, Speech, and Signal Processing '83*, volume 8, 332–335. 1983.

[6] Buckley, K.M. and Lloyd J. Griffiths. "Broad-band signal-subspace spatial-spectrum (BASS-ALE) estimation". *IEEE Transactions on Acoustics, Speech and Signal Processing*, 36(7):953–964, 1988.

[7] Coker, M. and E. Ferrara. "A new method for multiple source location". *IEEE International Conference on Acoustics, Speech, and Signal Processing '82*, volume 7, 411–415. 1982.

[8] Doron, M.A. and A.J. Weiss. "On focusing matrices for wide-band array processing". *IEEE Transactions on Signal Processing*, 40(6):1295–1302, 1992.

[9] Feng, Xian, Jianguo Huang, Qunfei Zhang, and Haiyan Wang. "A novel DOA estimation method and its focusing matrices for multiple wide-band sources". *Proceedings of the 2003 International Conference on Neural Networks and Signal Processing*, volume 2, 1306–1309 Vol.2. 2003.

[10] Grenier, Y. "Wideband source location through frequency-dependent modeling". *IEEE Transactions on Signal Processing*, 42(5):1087–1096, 1994.

[11] H. Qayyum, M. Ashraf. "Performance Comparison of Direction of Arrival Estimation Algorithms". *International Bhurban Conference on Applied Sciences and Technology*, 240–243. 2011.

[12] Haykin, S., D. J. Thomson, and J. H. Reed. "Spectrum Sensing for Cognitive Radio". *Proceedings of the IEEE*, 97(5):849 –877, May 2009.

[13] Hung, H. and Mostafa Kaveh. "Focussing matrices for coherent signal-subspace processing". *IEEE Transactions on Acoustics, Speech and Signal Processing*, 36(8):1272–1281, 1988.

[14] Kay, S. M. *Fundamentals of Statistical Signal Processing: Estimation Theory*. Prentice-Hall, 1993.

[15] Khan, Z.I., M.M. Kamal, N. Hamzah, K. Othman, and N. I. Khan. "Analysis of performance for multiple signal classification (MUSIC) in estimating direction of arrival". *IEEE International RF and Microwave Conference*, 524–529. 2008.

[16] M. Jansson, M. Viberg, B. Ottersten and A. L. Swindlehurst. "Optimal Subspace Techniques for DOA Estimation in the Presence of Noise and Model Errors". URL http://newport.eecs.uci.edu/~swindle/pubs/OptimalSubspaceTechniquesforDOA.pdf.

[17] Qianqian, Wu, Xu Chunxiu, Wu Muqing, and Gao Hu. "An improved spectrum sensing method based on multitaper-singular value decomposition in Cognitive radio". *2nd International Conference on Signal Processing Systems*, volume 1, V1–619–V1–623. 2010.

[18] Schmidt, R.O. "Multiple emitter location and signal parameter estimation". *IEEE Transactions on Antennas and Propagation*, 34(3):276–280, 1986.

[19] Semtech Wirless and Sensing Products. *AN1200.03 Application Note Frequency Hopping*, 2005.

[20] Sklar, B. *Digital Communications: Fundamentals and Applications*. Prentice-Hall, 2001.

[21] Stallings, W. *Data and Computer Communications*. Prentice-Hall, eighth edition, 2007.

[22] Su, Guaning and M. Morf. "The signal subspace approach for multiple wide-band emitter location". *IEEE Transactions on Acoustics, Speech and Signal Processing*, 31(6):1502–1522, 1983.

[23] Wang, H. and M. Kaveh. "Coherent signal-subspace processing for the detection and estimation of angles of arrival of multiple wide-band sources". *IEEE Transactions on Acoustics, Speech and Signal Processing*, 33(4):823–831, 1985.

[24] Wax, M., Tie-Jun Shan, and T. Kailath. "Spatio-temporal spectral analysis by eigenstructure methods". *IEEE Transactions on Acoustics, Speech and Signal Processing*, 32(4):817–827, 1984.

[25] Yucek, T. and H. Arslan. "A survey of spectrum sensing algorithms for cognitive radio applications". *IEEE Communications Surveys Tutorials*, 11(1):116–130, 2009.

REPORT DOCUMENTATION PAGE

Form Approved
OMB No. 0704–0188

1. REPORT DATE *(DD–MM–YYYY)*	2. REPORT TYPE	3. DATES COVERED *(From — To)*
27–03–2014	Master's Thesis	Aug 2012–Mar 2014

4. TITLE AND SUBTITLE

Multiple Signal Classification for Determining Direction of Arrival of Frequency Hopping Spread Spectrum Signals.

5a. CONTRACT NUMBER

5b. GRANT NUMBER

5c. PROGRAM ELEMENT NUMBER

6. AUTHOR(S)

Alsubaie, Fawwaz, First Lieutenant, Royal Saudi Air Force, RSAF

5d. PROJECT NUMBER

5e. TASK NUMBER

5f. WORK UNIT NUMBER

7. PERFORMING ORGANIZATION NAME(S) AND ADDRESS(ES)

Air Force Institute of Technology
Graduate School of Engineering and Management (AFIT/EN)
2950 Hobson Way
WPAFB, OH 45433-7765

8. PERFORMING ORGANIZATION REPORT NUMBER

AFIT-ENG-14-M-05

9. SPONSORING / MONITORING AGENCY NAME(S) AND ADDRESS(ES)

Intentionally left blank

10. SPONSOR/MONITOR'S ACRONYM(S)

11. SPONSOR/MONITOR'S REPORT NUMBER(S)

12. DISTRIBUTION / AVAILABILITY STATEMENT

DISTRIBUTION STATEMENT A:
APPROVED FOR PUBLIC RELEASE; DISTRIBUTION UNLIMITED

13. SUPPLEMENTARY NOTES

14. ABSTRACT

This research extends a MUSIC algorithm to determine DOA of FHSS signals. All incident FHSS signals have unknown DOA and use PSK. Conventional MUSIC algorithm involves multiple MUSIC estimation for all frequency bins. On the other hand, the extended development is meant to execute a single MUSIC algorithm of observations on multiple frequency bins or hops. The new extension shows better performance compared to the conventional MUSIC execution at different SNR levels. Both have the same power accumulation at the true angles of arrival. However, the new development has lower side lobes and hence helps avoid false detections. In addition, the new development has lower side lobes variance resulting in lower error of false detections compared to the normal execution. Simulation results show that the new extension is sensitive to the SNR values and number of samples taken at each frequency bin. However, it is less sensitive to the possible number of frequency hops or ***hop set*** and number of array sensors.

15. SUBJECT TERMS

MUSIC Algorithm, Direction of Arrival, Frequency Hopping Spread Spectrum, Communication, Estimation

16. SECURITY CLASSIFICATION OF:			17. LIMITATION OF ABSTRACT	18. NUMBER OF PAGES	19a. NAME OF RESPONSIBLE PERSON
a. REPORT	b. ABSTRACT	c. THIS PAGE			Dr. Richard K. Martin (ENG)
U	U	U	UU	75	19b. TELEPHONE NUMBER *(include area code)* (937) 2553636 x4625; Richard.Martin@afit.edu